Source-Channel Mappings with Applications to Compressed Sensing

by

Ahmad Abou Saleh

A thesis submitted to the
Department of Electrical and Computer Engineering
in conformity with the requirements for
the degree of Master of Science

Queen's University
Kingston, Ontario, Canada
July 2011

Abstract

Tandem source-channel coding is proven to be optimal by Shannon given unlimited delay and complexity in the coders. Under low delay and low complexity constraints, joint source-channel coding may achieve better performance. Although digital joint source-channel coding has shown a noticeable gain in terms of reconstructed signal quality, coding delay, and complexity, it suffers from the leveling-off effect. However, analog systems do not suffer from the leveling-off effect. In this thesis, we investigate the advantage of analog systems based on the Shannon-Kotel'nikov approach and hybrid digital-analog coding systems, which combine digital and analog schemes to achieve a graceful degradation/improvement over a wide range of channel conditions. First, we propose a low delay and low complexity hybrid digital-analog coding that is able to achieve high (integer) expansion ratios (≥ 3). This is achieved by combining the spiral mapping with multiple stage quantizers. The system is simulated for a $1:3$ bandwidth expansion and the behavior for a $1:M$ (with M an integer≥ 3) system is studied in the low noise level regime.

Next, we propose an analog joint source-channel coding system that is able to achieve a low (fractional) expansion ratio between 1 and 2. More precisely, this is an $N:M$ bandwidth expansion system based on combining uncoded transmission and a $1:2$

bandwidth expansion system (with $N < M < 2N$).

Finally, a $1 : 2$ analog bandwidth expansion system using the (Shannon-Kotel'nikov) Archimedes' spiral mapping is used in the compressed sensing context, which is inherently analog, to increase the system's immunity against channel noise. The proposed system is compared to a conventional compressed sensing system that assumes noiseless transmission and a compressed sensing based system that account for noise during signal reconstruction.

Acknowledgements

I would like to express my sincere thanks to my supervisors, Dr. Fady Alajaji and Dr. Wai-Yip Geoffrey Chan, for their support, continuous encouragement, and thoughtful suggestions and comments throughout the completion of this work.

I am indebted to my parents and brothers for their continuous encouragements and expectations. Finally, I would like to thank Dr. Shahram Yousefi, and Dr. Hossam Hassanein for serving in my thesis committee.

Contents

List of Figures

List of Acronyms

AWGN Additive White Gaussian Noise

BP Basis Pursuit

BPAM Block Pulse Amplitude Modulation

BPDN Basis Pursuit with Denoising

COVQ Channel-Optimized Vector Quantization

CS Compressed Sensing

CSNR Channel Signal-to-Noise Ratio

FC Fusion Center

HDA Hybrid Digital-Analog

HSQLC Hybrid Scaler Quantizer Linear Coder

MAP Maximum A Posteriori

ML Maximum Likelihood

MMSE Minimum Mean Square Error

MSE Mean Square Error

OPTA Optimal Performance Theoretically Attainable

PAM Pulse Amplitude Modulation

PCCOVQ Power Constrained Channel-Optimized Vector Quantization

SDR Signal-to-Distortion Ratio

TSNR Total Signal-to-Noise Ratio

Chapter 1

Introduction

Telecommunication is an increasingly important part of modern societies as it enables the transportation of information in a short time without being hindered by distance. One of the ultimate goals in communication systems is to provide highly reliable and efficient transmission of data bearing signals, such as text, images, video, speech, over a noisy medium (e.g., wireless channels). Such signals have a high information rate, while the medium has a limited capacity.

Source compression (source coding) and efficient use of the channel (channel coding) were subject to extensive research over the last decades. Despite great achieved progress, particularly vis-a-vis separate (tandem) source and channel coding, it is not always possible to reach the desired quality of the received signal under channel and complexity constraints. The combination of source and channel coding may achieve better performance under limited resources. Thus joint source-channel coding is a topic that is receiving increasing attention.

In this thesis, we investigate two different joint source-channel coding methods for the

reliable and efficient transmission of analog-valued sources over Gaussian channels. One is based on analog mapping and referred to as Shannon-Kotel'nikov mapping, and the other is based on hybrid digital-analog coding. Furthermore, we adapt and apply the use of Shannon-Kotel'nikov mapping within the compressed sensing context to increase the system's immunity against channel noise.

1.1 Source and Channel Coding

1.1.1 Tandem Coding System

Typically, in communication systems, sources are often modeled by a discrete-time continuous-amplitude (analog) random sequence. Due to bandwidth and storage restrictions, source sequence are usually compressed using a source encoder to remove its redundancy. This operation is referred to as *source coding*. The inevitable loss of information from source coding may lead to a greater level of sensitivity to channel noise. Hence, a channel encoder is required to add some controlled redundancy at the output of the source encoder for error protection. This operation, which is often called *channel coding*, can correct errors in addition to its ability to detect errors. To get an estimate of the source sequence, channel and source decoders are, respectively, applied on the noisy received channel encoder output. This communication system, that uses separately designed source and channel coders as shown in Fig. 1.1, is often called a *tandem coding system*.

According to Shannon, the rate distortion function $R(D)$ is the minimum rate needed

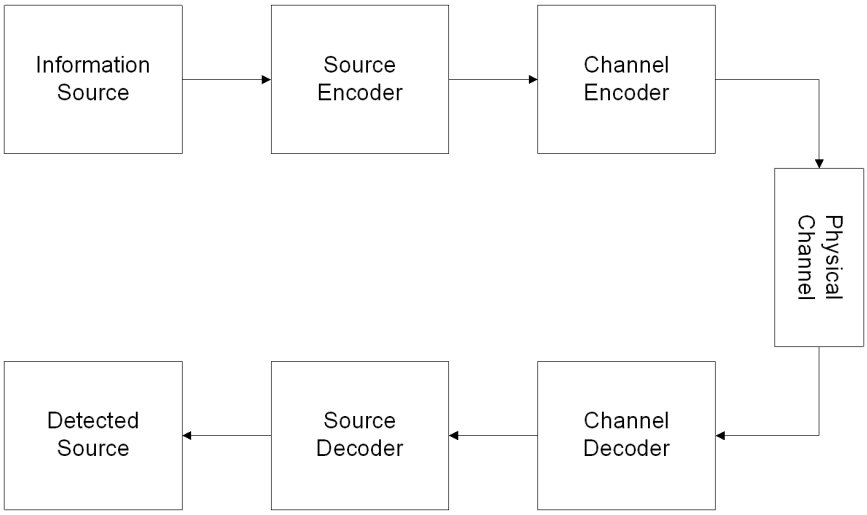

Figure 1.1: Block diagram of the tandem source-channel coding system.

to encode a source with an average distortion not exceeding D; and the capacity-cost function $C(P)$ is the maximum rate at which channel can transmit information reliably given an average power constraint P on the channel input. As a result, Shannon showed that a source signal can be transmitted (optimally) with fidelity D via a tandem coding scheme if $R(D) \leq C$. This result is known as the *source-channel separation theorem* [3, 4].

1.1.2 Joint Source-Channel Coding

There are a few problems with tandem systems that have motivated researchers to investigate joint source-channel coding. One main problem that is worth mentioning about the *source-channel separation theorem* is that the coders must have unlimited delay and complexity in order to achieve optimality. This means that, in practice, for delay and complexity constrained applications, the tandem system might not

be optimal. Another problem is that both source and channel coders are designed separately. This means that the source codes are designed assuming that the channel codes can correct all errors introduced by the channel noise, and the channel codes are designed to protect the source codes equally assuming the latter are uniformly distributed. These assumptions are not true in practice and indeed unequal error protection with source codes can achieve better performance. Another important drawback is that the separate source-channel system is highly non-robust. More specifically, if the true channel capacity is lower than the capacity of the designed channel, channel codes cannot give a low error rate, and the performance degrades drastically. This is often called the *threshold effect* [1]. Furthermore, if the true capacity is higher than the capacity of the designed channel, the performance does not improve beyond a certain threshold. This is referred to as the *leveling-off effect* [1].

Joint source-channel coding techniques include: (a) unequal error protection in which channel codes protect source information according to its level of importance ; (b) optimal quantizer design for noisy channels such as channel-optimized vector quantization (COVQ) [5]; (c) direct source-channel mapping [1, 6, 7, 8].

Although digital joint source-channel coding have shown a noticeable gain in terms of reconstructed signal quality, coding delay and complexity, it usually suffers from the leveling-off effect. This leads us to investigate the advantage of (1) analog systems (i.e., Shannon-Kotel'nikov mapping) that are based on the direct source-channel mapping technique and (2) hybrid digital-analog coding systems which combines digital and analog schemes to achieve a graceful performance for a wide range of channel conditions.

1.2 Compressed Sensing

Compressed sensing or *compressive sensing* (CS) refers to the problem of recovering a signal using fewer ("sparse") linear measurements. The conventional signal compression methodology is based on acquiring the entire signal (usually large), and then throwing away information during compression. This technique, which uses a lot of resources for data acquisition followed by compression, was questioned by Donoho [9] by raising a fundamental question: Is there a method that acquires the signal in a compressed manner and directly sense the essential part of the signal (i.e., combine the two process of acquiring and compressing)? Recent work on compressed sensing is continuously producing positive results in that direction.

As mentioned, the aim of CS is to reconstruct a signal from a set of few linear measurements. At first glance, it might be impossible to reconstruct a signal from an underdetermined (i.e., incomplete) set of measurements. However, considering sparse finite-dimensional signals, those with few nonzero coordinates, the reconstruction only depends on a number of degrees of freedom which is smaller than the signal dimensional space. Many signals such as real-world images, and audio signals, are sparse in some basis. These sparse signals, which lie in a lower dimensional space, may be represented with a fewer measurements. However, it might be difficult to determine in which lower dimensional subspace such signals lie. In the recent literature, several reconstruction algorithms have been developed to solve the sparse recovery problem. There are two main approaches to this problem. The first one is based on convex relaxation which can be solved using linear programming such as basis pursuit [10], whereas the second approach is based on iterative greedy search strategies such as matching pursuit [11].

Finally, for CS to be widely applicable, recovery algorithm should be stable. This is essential, since in practice, we often encounter noisy signals or measurements, and most real-world signals are not exactly sparse. This lead us to investigate Shannon-Kotel'nikov mapping, that acts as an analog joint source-channel encoder, within the CS context to increase immunity against channel noise.

1.3 Summary of Contribution

In this thesis, all studied systems are based on the $1:2$ double Archimedes' spiral mapping. First, we combine the spiral mapping with multiple stage quantizers to achieve high (integer) expansion ratios (≥ 3). Then, the uncoded and the spiral mappings are used to obtain a low (fractional) overall expansion ratio between 1 and 2. Finally, the $1:2$ spiral mapping is applied within the compressed sensing context to increase system's immunity against channel noise. The primary contributions of this thesis are summarized as follows:

- Minimum mean square error (MMSE) and maximum a posteriori (MAP) decoders are investigated with $1:2$ bandwidth expansion systems using the double Archimedes' spiral mapping. Using MMSE/MAP estimator instead of maximum likelihood (ML) is shown to achieve a graceful improvement/degradation over a wide range of noise levels.

- A $1:3$ joint source-channel coding system based on hybrid digital-analog scheme is proposed. The proposed scheme has a low delay/complexity since it encodes one source symbol at a time (no delay), and uses a scalar quantizer and a mapping function at the encoder side; the decoder is implemented using a quantizer

and a table-lookup. An upper bound on the end-to-end distortion is derived. The performance of the proposed hybrid system is investigated and compared to other reference systems. A generalization of the $1:3$ system to achieve higher expansion ratio $1:M$ (with M an integer bigger than 3) is proposed by using multiple stage quantizers. Furthermore, the behavior of this system is studied in the low noise level regime.

- A purely analog lossy joint source-channel coding system is presented. This system is based on combining an uncoded system and a $1:2$ bandwidth expansion system. As a result, the proposed system can achieve any overall expansion ratio between 1 and 2. Power is optimally allocated between the uncoded and the expansion systems in order to minimize the overall distortion.

- Shannon-Kotel'nikov mapping is applied on compressed sensing in the presence of noise. The proposed scheme is optimized for minimal end-to-end distortion. The proposed system is compared to two CS-based systems.

1.4 Thesis Overview

The thesis contains 6 chapters. The main ones are Chapters $3-5$.

In Chapter 2, a description of the general communication system is first given. The theoretical limit of such system is then presented. We further review various joint source-channel coding schemes including optimal linear systems, power constraint channel-optimized vector quantization, Shannon-Kotel'nikov mappings, and hybrid digital-analog systems. In addition, a detailed description of a $1:2$ Shannon-Kotel'nikov system based on the double Archimedes' spiral mapping is presented.

Furthermore, MMSE and MAP decoders are assessed on this system instead of ML decoder used previously.

In Chapter 3, a hybrid digital-analog source-channel coding with $1:3$ bandwidth expansion is proposed. The system parameters are numerically optimized to minimize a target distortion. The performance of the $1:3$ bandwidth expansion system is investigated and compared to other reference systems. Moreover, an upper bound on the end-to-end system distortion is derived. Furthermore, we generalize the system to achieve higher expansion ratios $1:M$ (where $M > 3$) in which its behavior in the CSNR limit is studied.

In Chapter 4, a purely analog joint source-channel coding is presented. This system is an $N:M$ bandwidth expansion scheme as long as the condition $N < M < 2N$ is fulfilled. Power is optimally allocated to minimize the overall distortion.

In Chapter 5, a $1:2$ Shannon-Kotel'nikov mapping is applied within the compressed sensing context to increase the CS system's immunity against channel noise. The number of measurements is optimized to minimize the overall MSE distortion. The proposed scheme is compared with a CS-based system which accounts for channel noise during signal reconstruction.

Finally, conclusions are presented in Chapter 6.

Chapter 2

Preliminaries

2.1 General Problem Formulation

We consider the problem of transmitting a discrete-time, continuous-amplitude source over a memoryless discrete-time, continuous-amplitude channel. We assume that the channel symbols are corrupted by an additive white Gaussian noise (AWGN). This communication system is illustrated in Fig. 2.1. The source symbol X is encoded to generate the channel input symbol Y. After transmission, the channel input is corrupted by noise W resulting in channel output $\hat{Y} = Y + W$, where W is drawn from an independent and identically distributed (i.i.d.) Gaussian process with mean zero and variance σ_W^2 ($W \sim \mathcal{N}(0, \sigma_W^2)$). At the receiver side, the channel output $\hat{Y}$ is decoded to produce an estimate of the source symbol $\hat{X}$.

The aim in such communication system is to reconstruct the estimate source symbol $\hat{X}$ with some fidelity criterion. The distortion measure that is considered in this thesis

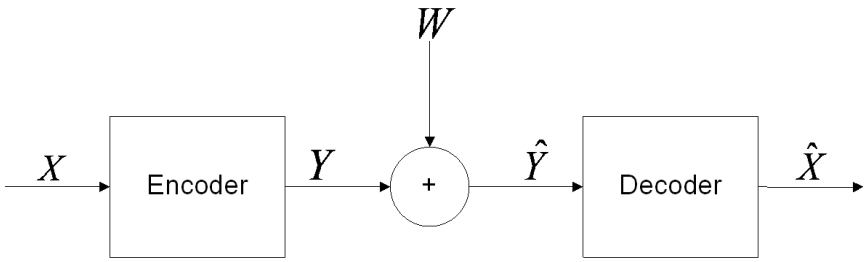

Figure 2.1: A general point-to-point communication system.

is the mean square error (MSE)

$$d(X, \hat{X}) = (X - \hat{X})^2. \tag{2.1}$$

The general system design can be formulated by finding the encoder and the decoder that minimize the average distortion

$$D = \mathbb{E}[d(X, \hat{X})] = \int \int (x - \hat{x})^2 f_{X,\hat{X}}(x, \hat{x}) dx d\hat{x} \tag{2.2}$$

where $\mathbb{E}[.]$ denotes the expectation operator, and $f_{X,\hat{X}}(x, \hat{x})$ is the joint probability density function (pdf) of the source symbol and the reconstructed one. The minimization of (2.2) should be done under a transmission power constraint P

$$\mathbb{E}[Y^2] = \int y^2 f_Y(y) dy \leq P \tag{2.3}$$

where $f_Y(y)$ is the pdf of the channel input Y.

2.2 Theoretical Limit

In this section, we present the theoretical limit of the communication problem. We limit our discussion to the theoretical lower bound on the distortion for the case of the memoryless Gaussian source and the AWGN channel. Note that the definition of this bound is based on the fundamental source and channel separation theorem introduced by Shannon [3].

2.2.1 Bounds on Source-Channel Coding

Fig. 2.2 shows the block diagram of a tandem source-channel coding system. In this system, samples of the source are grouped into blocks of size N; a source encoder that compress the source information and a channel encoder that protect the source information from channel noise by adding some controlled redundancy are applied to the source vector $\mathbf{X}^N$ in order to produce the channel input $\mathbf{Y}^M$, where M is the number of channel symbols. At the receiver side, both channel and source decoder are applied to estimate the information source.

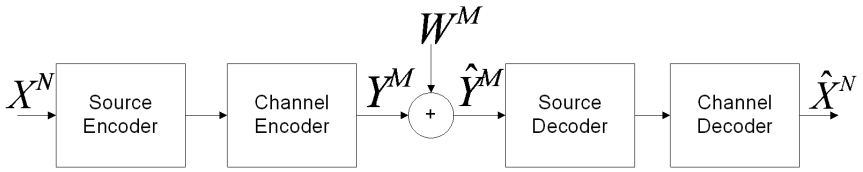

Figure 2.2: A point-to-point communication system based on the separation theorem.

Given a fidelity criterion, Shannon derived an absolute lower bound on the rate of the source. This is known as the rate-distortion function. For a memoryless (i.i.d.)

Gaussian source X under the MSE distortion measure, the rate-distortion function can be expressed as follows [4]

$$R(D) = \max\left[\frac{1}{2}\log\left(\frac{\sigma_X^2}{D}\right), 0\right] \quad \text{(bits/source symbol)} \tag{2.4}$$

where σ_X^2 is the source signal power, and D is the distortion.

Moreover, information from source encoder is transmitted over a noisy medium (channel). The channel capacity represents an upper limit on the rate at which information can be transmitted reliably (with probability of error that asymptotically vanishes with respect to the coding blocklength) given a certain channel signal-to-noise ratio (CSNR) [3]. For the AWGN channel with an average power constraint P on the channel input, the capacity-cost function is given by [4]

$$C(P) = \frac{1}{2}\log\left(1 + \frac{P}{\sigma_W^2}\right) \quad \text{(bits/channel use)} \tag{2.5}$$

where the ratio P/σ_W^2 is the CSNR.

2.2.2 Optimal Performance Theoretically Attainable

As a result of the definition of the rate-distortion and capacity-cost functions, a memoryless source that can be reproduced (at an overall rate of M/N channel use per source symbol) at the receiver side of a memoryless channel with power constraint P and distortion at most D requires that its rate-distortion $R(D)$ is less than or equal to the capacity of the channel $C(P)$. Furthermore, it was shown by Shannon that the source can be asymptotically reproduced at the receiver side with fidelity distortion

at most D via a tandem code if $R(D) \leq C(D)$. Hence, for the memoryless Gaussian source-channel pair, the optimal performance theoretically attainable (OPTA) can be found by equating the source rate and the channel capacity ($NR(D) = MC(P)$) as follows

$$\text{SDR} \triangleq \frac{\sigma_X^2}{D} = \left(1 + \frac{P}{\sigma_W^2}\right)^{M/N} \tag{2.6}$$

where SDR is the signal-to-distortion ratio. When $M > N$, redundant dimension is available and error correction can be used; and when $N > M$, the source has to be compressed to lower dimension before transmission.

2.3 Joint Source-Channel Coding Schemes

In order to implement a mapping from a source symbol of bandwidth B_S to a channel symbol of bandwidth B_C, we will use the block-based approach as shown in Fig. 2.3. In this system, samples of the memoryless source X are grouped into blocks of size N and encoded using $\gamma(.)$. The encoder maps the source vector $\mathbf{X}^N$ to an input channel vector $\mathbf{Y}^M$ of length M. By having $M/N = B_C/B_S$, bandwidth expansion/reduction is obtained by mapping the N source samples into M channel samples. Note that bandwidth expansion/reduction and dimension expansion/reduction are used interchangeably in this thesis.

2.3.1 Optimal Linear System

Block pulse amplitude modulation (BPAM) is the optimal (in the mean square sense) linear system for transmitting a vector source on a vector channel with additive noise

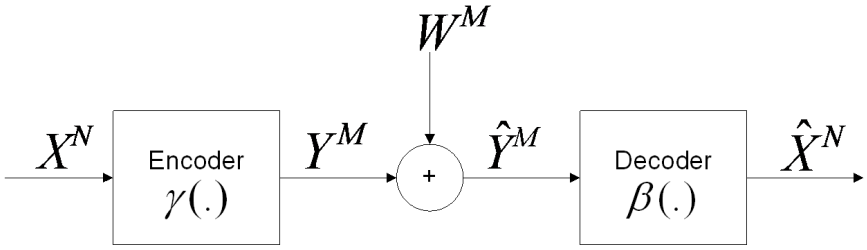

Figure 2.3: A point-to-point block-based system.

[2]. Assume that an i.i.d. N dimensional Gaussian source $\mathbf{X}^N$ is to be transmitted by means of a M dimensional channel vector $\mathbf{Y}^M$. In [2], it was shown that when $N < M$ (bandwidth expansion), the transmitter and the receiver that minimize the MSE distortion under an average power constraint P are given by

$$\mathbf{Y}^M = \alpha(\mathbf{X}^N) = \mathbf{T}\mathbf{X}^N \quad \text{and} \quad \hat{\mathbf{X}}^N = \beta(\mathbf{Y}^M) = \mathbf{R}\hat{\mathbf{Y}}^M \tag{2.7}$$

where $\hat{\mathbf{Y}}^M = \mathbf{Y}^M + \mathbf{W}^M$ is the received signal, $\mathbf{T}$ and $\mathbf{R}$ are respectively the encoder and decoder matrices

$$\begin{aligned} \gamma &\triangleq \mathbf{T} = \sqrt{\frac{M}{N}}\frac{\sqrt{P}}{\sigma_X}\mathbf{I}_{M\times N} \\ \beta &\triangleq \mathbf{R} = \sqrt{\frac{N}{M}}\frac{\sqrt{\sigma_X^2 P}}{P+\sigma_W^2}\mathbf{I}_{N\times M} \end{aligned} \tag{2.8}$$

where $\mathbf{I}_{N\times M}$ is a $N \times M$ matrix with ones on the main diagonal and zeros elsewhere. On the other hand, when $N > M$ (bandwidth reduction), the linear system's transmitter and receiver matrices can be expressed as follows

$$\begin{aligned} \mathbf{T} &= \frac{\sqrt{P}}{\sigma_X}\mathbf{I}_{M\times N} \\ \mathbf{R} &= \frac{\sqrt{\sigma_X^2 P}}{P+\sigma_W^2}\mathbf{I}_{N\times M}. \end{aligned} \tag{2.9}$$

In effect, the optimal linear system inserts zero samples when more channel bandwidth is available ($M > N$) and removes source samples when channel bandwidth is limited ($M < N$). Fig. 2.4 shows the performance of the optimal linear system for a $1:2$ bandwidth expansion ratio (i.e., $N = 1$, $M = 2$) and $2:1$ bandwidth reduction. The $1:1$ theoretical limit is also shown for comparison. The plot is made for a memoryless Gaussian source X with unit variance. From Fig. 2.4, we can notice that when using a linear system for dimension reduction, the system performance saturates at some point. This can be explained in a similar way to the leveling-off effect in a purely digital system. In addition to that, it is clear that the linear system is closest to the optimal performance at low CSNR levels; however as CSNR increases, the linear system is far from optimal. Moreover, in [2], the authors have proven that BPAM approaches OPTA when CSNR goes to $-\infty$. Hence, the linear system performs well for a very poor channels which is usually not of interest. This motivates the investigation for other schemes that can achieve better performance such as non-linear systems.

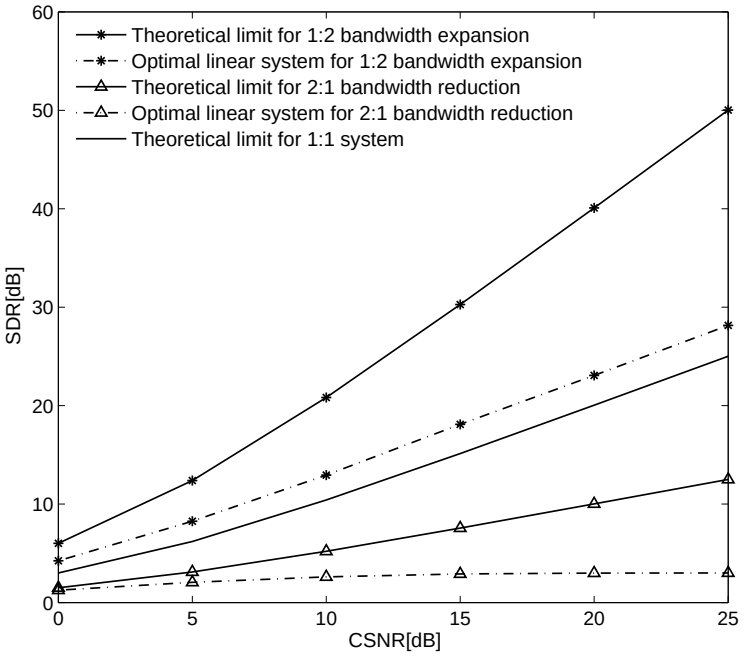

Figure 2.4: Performance of the optimal linear system for different dimension expansion/reduction ratios. The theoretical limit (OPTA) is also plotted for comparison. The plot is for a memoryless Gaussian source with unit variance.

2.3.2 Power Constrained Channel-Optimized Vector Quantization

The power constrained channel-optimized vector quantization (PCCOVQ) is proposed in [12, 13]. The approach used follows the framework of the block-based system shown in Fig. 2.3. Here again, the objective is to find the encoder γ and the decoder β that minimize the average MSE distortion $D(\gamma, \beta) = \mathbb{E}[||\mathbf{X}^N - \hat{\mathbf{X}}^N||^2]/N$ subject to an average transmission power $P(\gamma) = \mathbb{E}[||\gamma(\mathbf{X}^N)||^2]/M \leq P$. Using the Lagrangian method, the constrained optimization problem can be recast into an unconstrained

minimization problem given by

$$\min_{\gamma,\beta}[D(\gamma,\beta)+\lambda P(\gamma)] \tag{2.10}$$

where λ is the Lagrange multiplier used to control the average power. Note that this problem is related to the COVQ design problem but with an additional constraint on the transmission power.

At the encoder side, the authors in [12, 13] propose to use a vector quantizer followed by a mapping from the source space to a finite channel space set. The channel signal set is an M-fold cartesian product of a uniform pulse amplitude modulation (PAM) alphabet. The receiver side uses a nearest neighbor detector to choose the decoded source from a reconstruction codebook. The encoder partition, the reconstruction codebook, and the distance between samples in the channel signal set are optimized to minimize the MSE distortion under a power constraint. This is done using a modified generalized Lloyd algorithm.

Both bandwidth reduction ($N > M$) and expansion ($N < M$) are developed in [13]. It is shown that PCCOVQ performs well for dimension reduction; there is only 1 dB gap between the SDR performance of a $2:1$ PCCOVQ and the theoretical limit OPTA. However, for bandwidth expansion, PCCOVQ does not perform well with respect to other reference systems. In [14], the authors focus on PCCOVQ for bandwidth expansion. They apply the same algorithm as the one proposed in [13] but using different initial conditions and a larger number of samples in the channel signal set. These slight modifications are shown to improve the performance of the PCCOVQ for bandwidth expansion. Simulation results indicate that the performance of $1:2$ and $1:3$ PCCOVQ systems are comparable to other state of the art reference

systems [14]. However, it is important to note that due to the use of a large number of symbols in the channel signal set, the computational complexity for the system design will get large as the expansion ratio and the CSNR level increase [14].

In Fig. 2.5, we show the reconstruction codebook of size 512 for a 2 : 1 PCCOVQ. Notice that for low CSNR (0 dB), the codebook gives a straight line shape which is similar to the linear system (BPAM). In BPAM, we disregard one component and hence the mapping is a line along one of the axes. For high CSNR (20 dB), the codebook has a similar shape to a double Archimedes' spiral.

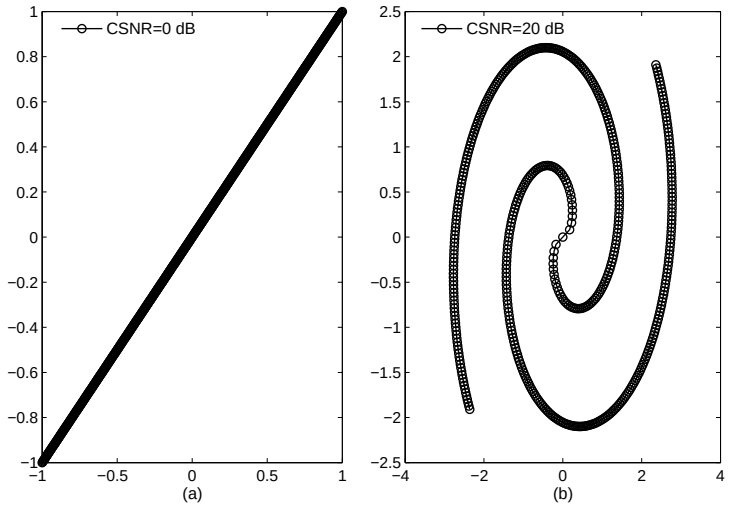

Figure 2.5: The reconstruction codebook of size 512 for a 2 : 1 PCCOVQ system. The system is designed for (a) CSNR = 0 dB and (b) CSNR = 20 dB. The graph is made for an i.i.d. Gaussian source with unitary variance.

2.3.3 Shannon-Kotel'nikov Mappings

As opposed to quantizing the source into a discrete set of representation points which are then mapped into the channel space, Shannon-Kotel'nikov mapping [1, 15] is an approach based on direct source-channel mapping in which source and channel coders are combined into one mathematical operation. This operation maps the source space directly into the channel space. The main idea is based on a geometrical characterization of the communication problem in which the source is represented using a point in the source space $\mathbb{R}^N$ (*message space*), and the channel input is a point in the channel space $\mathbb{R}^M$ (*signal space*). This approach is introduced by Shannon in [1]. Furthermore, Kotel'nikov presents a theory for bandwidth expansion in his doctoral dissertation [15] by using a similar signal mapping approach; and hence its name.

Shannon-Kotel'nikov mappings perform either a projection of the source onto a lower dimensional space or map the source into a higher dimensional space. The former represents a lossy compression of the source (system bandwidth reduction), while the latter uses the redundant dimensions for error control (system bandwidth expansion). In the case of a match between the source and the channel bandwidth (i.e., same dimension), it is well known that a linear, or uncoded, transmission is optimal [16]. However, when the source and channel dimensions are not equal, linear transmission is suboptimal as was previously discussed in Section 2.3.1. Instead of discarding the excess of source samples to achieve bandwidth reduction, or repeating part of the source samples for bandwidth expansion, nonlinear mapping needs to be explored in order to achieve a better performance.[1] In [1], Shannon proposed a similar mapping as

[1]Note that repeating part of the source or inserting zeros samples will not alter the performance

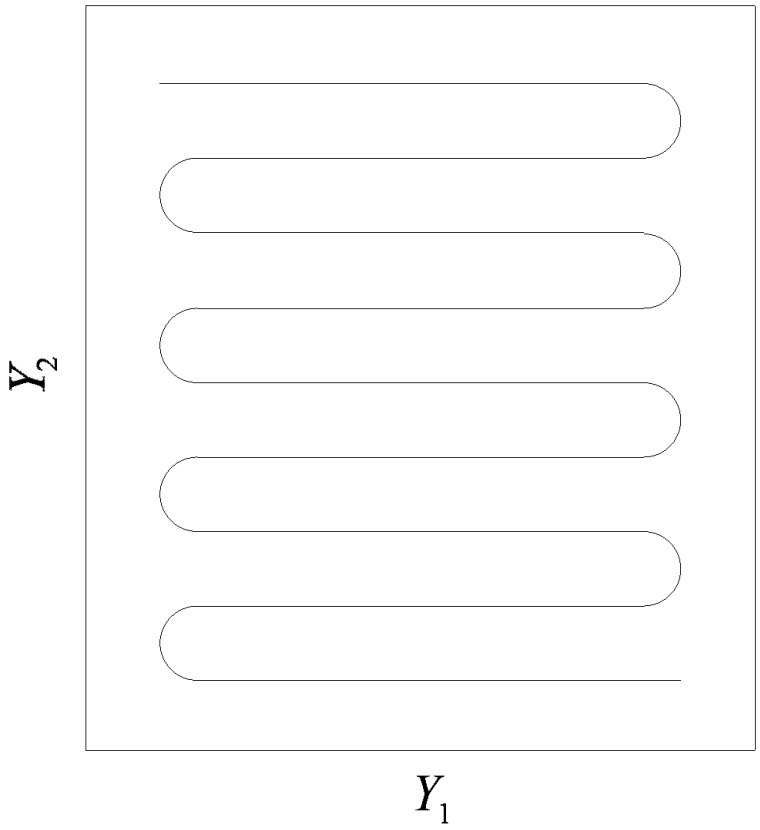

Figure 2.6: Shannon's example on 1 : 2 dimension expansion mapping [1].

that shown in Fig. 2.6 as an example to achieve a 1 : 2 bandwidth expansion. In this mapping, the one-dimensional source is given by the line space (e.g., the length along the curve) which is mapped to a two-dimensional channel input using (Y_1, Y_2). This approach will perform better than just sending twice the same source symbol and do averaging at the decoder side. Shannon also suggested that the same mapping shown in Fig. 2.6 can be used for bandwidth reduction by interchanging the source and the channel space. This is done by projecting every source vector (X_1, X_2) into the nearest point on the mapping curve which will be represented using a one-dimensional

of the system since both mapping are related by some orthonormal transformation.

channel space (e.g., the distance from some reference origin to the projected point on the curve).

Since the Shannon-Kotel'nikov approach uses space filling curves to perform the source-to-channel space mapping, one main question is: How one can determine the optimal geometrical structure of the mapping? One way is to look at the codebook structure of the PCCOVQ [12, 13] which is closely related to Shannon-Koteln'nikov approach. By connecting the adjacent codebook points of the PCCOVQ, we can obtain a space filling-curve that can be used as a mapping function.

Another way is to search for a mapping function that satisfies some necessary requirements [8]: 1) The curve should cover well the entire source space to reduce overload distortion; 2) source symbols with high probability have to be mapped to low power channel symbols to minimize the transmission power; 3) points in the channel space that are close to each other must be mapped to source symbols that are also close in the source space in order to minimize distortion. Moreover, for bandwidth expansion, it is important to design the mapping such that channel representations have a low correlation so that no redundant information is transmitted on different channel symbols.

In [17, 18, 19, 20], the authors have shown that for a memoryless Gaussian source, the double Archimedes' spiral is a good mapping for applying both $1:2$ bandwidth expansion and $2:1$ bandwidth reduction. As shown in Fig. 2.5, the reconstruction codebook for a $2:1$ PCCOVQ system designed for high CSNR levels resembles the spiral mapping. In this case, the advantage of using a parameterized Shannon-Kotel'nikov mapping is the easiness in designing the system for a given source and channel characteristics. This is done by only modifying the parameters of the mapping

so that the shape can be changed accordingly.

2.3.4 Hybrid Digital-Analog Systems

One of the main advantages of digital lossy communication systems is the ability to achieve asymptotically the theoretical performance for a given CSNR via the separate source-channel coding (tandem system). However, there are two main disadvantages with tandem systems. One is the *threshold effect* which means that the performance degrades drastically when the true CSNR is lower than the designed one. The other drawback is the *leveling-off effect* which means that the performance remains constant beyond a certain level even if the CSNR is increased. This is due to the non-recoverable distortion introduced by the quantizer.

The threshold effect can be solved using a digital joint source-channel coding. Such systems, however, do not solve the leveling-off effect. On the other hand, an analog system does not suffer from the leveling-off effect. This provides a motivation to exploit the advantage of both digital and analog systems by allowing part of the system to use digital modulation and coding and another part to use analog signaling.

Schemes based on hybrid transmission are built by splitting the source into a quantized (digital) part, and a quantization error (analog) part. A general block diagram of a hybrid digital-analog (HDA) system is shown in Fig. 2.7 [21, 22, 23, 24, 25, 26].

In [23], an HDA system for bandwidth expansion is built based on vector quantization and linear (uncoded) transmission. A design algorithm for the system optimization is also presented. In [22], a bandwidth expansion/reduction system using HDA is given. This system uses a tandem scheme using a turbo code in the digital part and a linear/non-linear mappings in the analog part. Note that the schemes in [22, 23] can

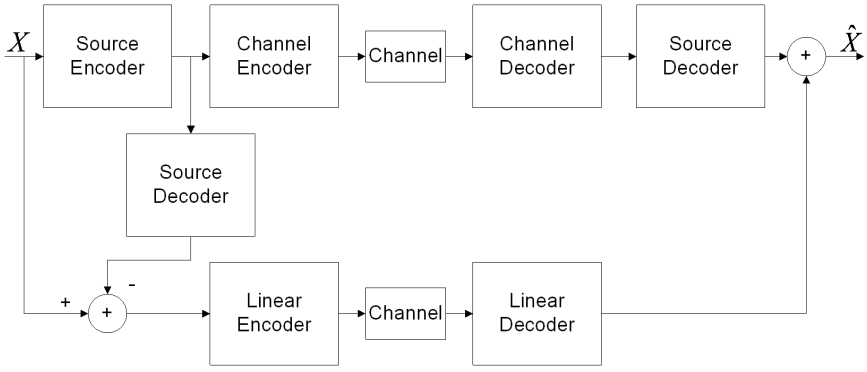

Figure 2.7: A block diagram of a general hybrid digital-analog system. The digital part uses a tandem scheme and the analog part uses a linear transmission.

achieve any expansion/reduction ratio. In [24, 25], a hybrid scheme which is referred to as hybrid scalar quantizer linear coder (HSQLC) is proposed. This scheme is able to achieve a $1 : 2$ bandwidth expansion by using a scalar quantizer in the digital part and a linear mapping in the analog part. Note that the HSQLC system has a low delay/complexity constraint since it encodes a single source sample at a time (no delay), and uses a simple scalar quantizer and a linear coder. In contrast, the previously mentioned HDA schemes use either a vector quantization or a tandem system (with powerful channel coding) in the digital part and hence incurs large delay and complexity.

In general, HDA systems have shown to offer a robust and graceful performance improvement/degradation for a wide range of CSNRs which make them suitable in many practical applications including broadcasting.

2.4 Improved 1:2 Bandwidth Expansion System

In this section, we focus on a 1 : 2 bandwidth expansion analog system using the Shannon-Kotel'nikov approach, where each source sample is represented as a point in a two-dimensional channel space. The double Archimedes' spiral mapping proposed in [17] is used. MMSE and MAP decoding are proposed to recover the source instead of ML decoding as used in [17]. Although ML decoder is simple and performs well at high CSNR levels [27, pp. 291-292], it is not optimal for the MSE distortion criterion and it is shown to give a poor performance at low CSNRs. MMSE decoding was proposed in [28] for bandwidth reduction. Here we will assess the use of both MMSE and MAP decoding with dimension expansion and compare it to the ML decoder.

2.4.1 System Model

Encoder

For an i.i.d. Gaussian source $X \sim \mathcal{N}(0, \sigma_X^2)$ and AWGN channel $W \sim \mathcal{N}(0, \sigma_W^2)$, the double Archimedes' spiral is a suitable mapping for a 1 : 2 bandwidth expansion [17]. Bandwidth expansion is performed by mapping each source sample $x \in \mathbb{R}$ to a two-dimensional channel symbol, which is a point on the double Archimedes' spiral shown in Fig. 2.8 and given by [17]

$$\mathbf{s}(x) = \begin{bmatrix} y_1(x) \\ y_2(x) \end{bmatrix} = \frac{1}{\pi} \begin{bmatrix} sgn(x)\Delta\varphi(x)\cos\varphi(x) \\ sgn(x)\Delta\varphi(x)\sin\varphi(x) \end{bmatrix} \tag{2.11}$$

where $sgn(\cdot)$ is the signum function, Δ is the radial distance between any two neighboring spiral arms, and $\varphi(x) = \sqrt{6.25|x|/\Delta}$. The radial distance Δ is the only

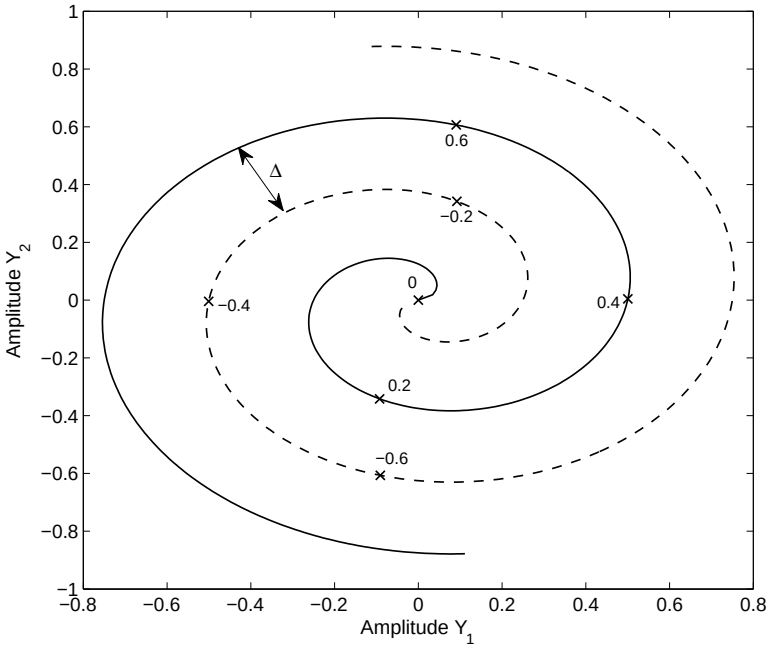

Figure 2.8: Double Archimedes' spiral. The negative source samples are mapped to the dashed line, whereas the positive ones are mapped to the solid line. The graph is plotted for $\Delta = 0.25$. The amplitude of the one-dimensional symbol is proportional to the length along the spiral arm from the origin to the mapped point. Some examples of the mapping are also plotted.

parameter that needs to be optimized in order to minimize the overall MSE distortion from using spiral mapping. Note that as shown from Fig. 2.8, equal increments in x correspond to equal increments in distance measured along the spiral curve.

Decoder

ML decoding

Given the received noisy two-dimensional channel output vector $\hat{\mathbf{Y}} = \mathbf{Y} + \mathbf{W}$, the ML estimate is given by the source x that maximizes the likelihood function

$$f_{\hat{\mathbf{Y}}|X}(\hat{\mathbf{y}}|x) = \left(\frac{1}{2\pi\sigma_W^2}\right) e^{-\frac{||\hat{\mathbf{y}}-\mathbf{y}||^2}{2\sigma_W^2}}. \tag{2.12}$$

This is achieved by the value x that minimizes the L_2 norm $||\hat{\mathbf{y}} - \mathbf{y}||$. Hence, the estimated source symbol corresponds to the point on the curve that is closest to the received point in the Euclidean norm. Although ML decoding is simple and performs well at high CSNRs, it is not optimal for the MSE distortion criterion. Next, we will describe the MMSE decoder, which is optimal, and the MAP decoder.

MMSE Decoding

In the mean square sense, the MMSE decoder is optimal and can be expressed as follows

$$\begin{aligned} \hat{x}_{\text{MMSE}} = \mathbb{E}[X|\hat{y}_1, \hat{y}_2] &= \int x f_{X|\hat{Y}_1,\hat{Y}_2}(x|\hat{y}_1, \hat{y}_2)dx \\ &= \frac{\int x f_{\hat{Y}_1,\hat{Y}_2|X}(\hat{y}_1, \hat{y}_2|x) f_X(x)dx}{\int f_{\hat{Y}_1,\hat{Y}_2|X}(\hat{y}_1, \hat{y}_2|x) f_X(x)dx}. \end{aligned} \tag{2.13}$$

For i.i.d. Gaussian noise, $f_{\hat{Y}_1,\hat{Y}_2|X}(\hat{y}_1, \hat{y}_2|x) = f_{\hat{Y}_1|X}(\hat{y}_1|x) f_{\hat{Y}_2|X}(\hat{y}_2|x)$, where

$$f_{\hat{Y}_i|X}(\hat{y}_i|x) = \frac{1}{\sqrt{2\pi}\sigma_W} e^{-\frac{(\hat{y}_i - y_i)^2}{2\sigma_W^2}}, \quad i = 1, 2 \tag{2.14}$$

and $y_i(x)$ is given by (2.11). Note that (2.13) is numerically calculated by discretizing x using a uniform quantization step d and calculating the mapped value $(y_1(x), y_2(x))$ for each discretized point. This gives a discretized version of each probability and the integration is simplified to only multiplication and addition operations. Note that this approximation is assumed to be good as long as the cardinality of the discrete set is sufficiently large and d is small in relation to the standard deviation of the channel noise.

Moreover, to make the decoder implementation computationally efficient, we devise a decoder based on quantization and table-lookup, thereby avoiding to perform a numerical integration for each received sample. This is achieved via uniform quantization of the output of the channel $\hat{\mathbf{y}} \in \mathbb{R}^2$ and looking up the decoded value $\hat{x}$ for each quantization bin in a table.

MAP Decoding

Here we exploit the use of the MAP decoder. MAP decoding is given by

$$\begin{aligned} \hat{x}_{\text{MAP}} &= \arg\max_x f_{X|\hat{Y}_1,\hat{Y}_2}(x|\hat{y}_1,\hat{y}_2) = \arg\max_x \frac{f_X(x) f_{\hat{Y}_1,\hat{Y}_2|X}(\hat{y}_1,\hat{y}_2|x)}{f_{\hat{Y}_1,\hat{Y}_2}(\hat{y}_1,\hat{y}_2)} \\ &= \arg\max_x f_X(x) f_{\hat{Y}_1,\hat{Y}_2|X}(\hat{y}_1,\hat{y}_2|x). \end{aligned} \tag{2.15}$$

In a similar way to the MMSE decoder, MAP decoder can be also applied using a quantizer and a table-lookup.

2.4.2 System Optimization

For a given CSNR, the radial distance Δ is the only parameter that needs to be optimized in order to minimize the overall MSE distortion [17]. When a received vector is decoded, we may encounter two types of error: 1) the threshold noise which occurs when choosing the wrong spiral arm; 2) and the weak noise which occurs when noise makes the estimated source sample to fall on the same spiral arm. Two examples that illustrate both weak and threshold distortion are shown in Fig. 2.9. When considering weak noise, the signal curve $\mathbf{s}$ can be approximated in the vicinity

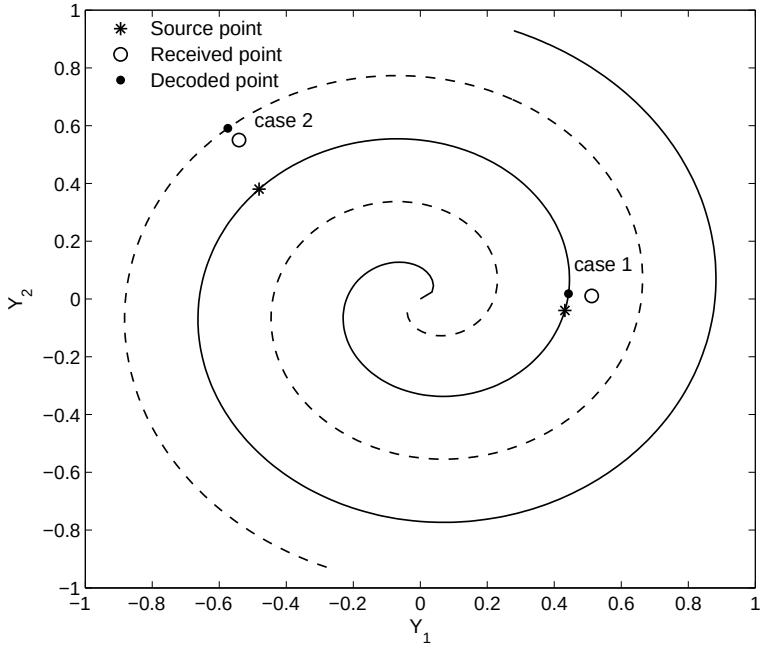

Figure 2.9: Cases 1 and 2 illustrate the weak noise and threshold distortion, respectively.

of a transmitted signal x_0 by (linear approximation) [17]

$$\mathbf{s}(x) \approx \mathbf{s}(x_0) + \mathbf{s}'_{\mathbf{0}}(x - x_0) \tag{2.16}$$

where $\mathbf{s'}_0 = \frac{d\mathbf{s}(x)}{dx} \mid_{x=x_0}$. The ML estimate of x can be approximated as the projection onto the tangent line through $\mathbf{s}(x_0)$ on the signal curve. Hence, the reconstructed sample $\hat{x}_{\mathrm{ML}}$ corresponds to the point on the curve given by

$$\mathbf{s}(\hat{x}_{\mathrm{ML}}) = \mathbf{s}(x_0) + \frac{< \mathbf{w}, \mathbf{s'}_0 >}{||\mathbf{s'}_0||^2}\mathbf{s'}_0 \tag{2.17}$$

where $< ., . >$ denotes the inner product operator. Comparing (2.16) and (2.17), the MSE distortion given that x_0 was transmitted, can be expressed as follows [17]

$$\begin{aligned} \varepsilon^2_{\mathrm{wn}} &= \mathbb{E}[(\hat{x}_{\mathrm{ML}} - x)^2 | x = x_0] = \frac{\mathbb{E}[< \mathbf{w}, \mathbf{s'}_0 >^2]}{||\mathbf{s'}_0||^4} \\ &= \frac{\sigma^2_W}{||\mathbf{s'}_0||^2} \end{aligned} \tag{2.18}$$

where the last equality is valid for Gaussian noise. The average weak noise MSE is then given by

$$\bar{\varepsilon}^2_{\mathrm{wn}} = \sigma^2_W \int \frac{1}{||\mathbf{s}'(x)||^2} f_X(x) dx. \tag{2.19}$$

From (2.19), one can observe that the norm of the tangent vector of $\mathbf{s}$ appears in the denominator. Hence, the longer these vectors are, the smaller the weak noise. Increasing the length without violating the transmission power constraint (i.e., without leaving a specified hyper-sphere), requires bending the curve. However, it is impossible to do that without increasing the threshold distortion. From Fig. 2.10, we can

notice how the power constraint which is illustrated using the dashed circle will increase the probability of having a threshold distortion from twisting and elongating the mapping function.

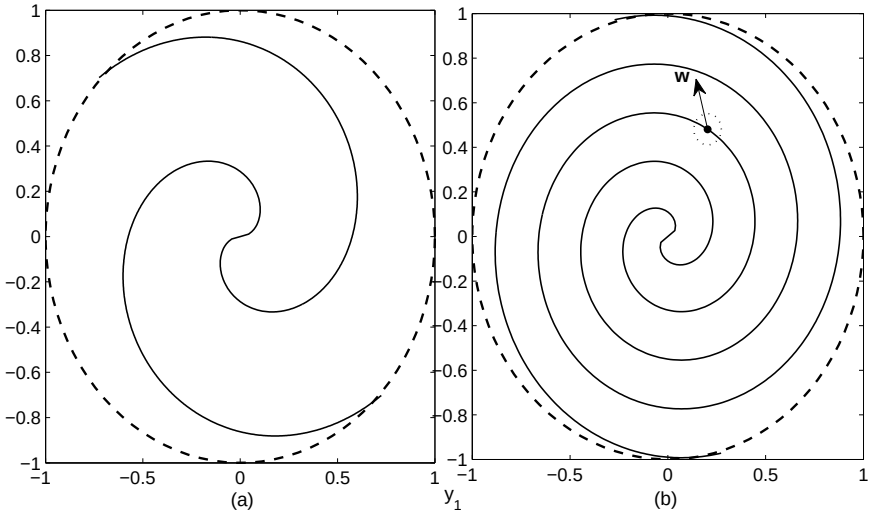

Figure 2.10: 1 : 2 dimension expansion using Archimedes' spiral. The big dashed circle shows the constraint region due to power constraint. (b) The same mapping of part (a) has been stretched to lower the weak noise however this will introduce threshold noise as shown from the noise vector **w**. The small dotted circle around the dotted source sample shows a region in which weak noise can occur.

Hence, for the spiral mapping, threshold distortion decreases when increasing Δ, whereas weak noise increases. The optimal Δ that minimizes the total distortion can be found by solving the following unconstrained optimization problem

$$\Delta_{\text{opt}} = \arg\min_{\Delta}[\bar{\varepsilon}^2_{\text{wn}}(\Delta) + \bar{\varepsilon}^2_{\text{th}}(\Delta)] \tag{2.20}$$

where $\bar{\varepsilon}^2_{\text{wn}}$ and $\bar{\varepsilon}^2_{\text{th}}$ are, respectively, the average weak noise and threshold distortion. From (2.11), $||\mathbf{s}'(\alpha x_0)||^2 = \alpha^2$, hence the average weak noise distortion can be expressed as follows [17]

$$\bar{\varepsilon}^2_{\text{wn}} = \frac{\sigma^2_W}{\alpha^2} \tag{2.21}$$

where α is a gain factor related to the average channel power constraint P via

$$P = \frac{1}{2}\int ||\mathbf{s}(\alpha x)||^2 f_X(x)dx. \tag{2.22}$$

The threshold distortion is calculated according to Fig. 2.11. Due to symmetry, it is sufficient to calculate the threshold distortion for one of the spiral arms, and then multiplying the result by 2.

Considering the positive spiral arm, the threshold distortion is calculated as follows [17]

$$\bar{\varepsilon}^2_{\text{th}} = 2Pr\int[(x-\hat{x}_+)^2 + (x-\hat{x}_-)^2]f_X(x)dx \tag{2.23}$$

where $\hat{x}_\pm$ are the reconstructed values when the threshold effect occur and Pr is the probability of a threshold distortion to occur [17]

$$Pr = \frac{1}{2}\left[1 - \text{erf}\left(\frac{\Delta}{2\sqrt{2}\sigma_W}\right)\right] \tag{2.24}$$

where erf$(\cdot)$ is the Gaussian error function. Note that the value that one get when the threshold effect occurs is the one corresponding to the point on the curve in radial distance Δ from the source point. In order to find the reconstructed values $\hat{x}_\pm$, it is

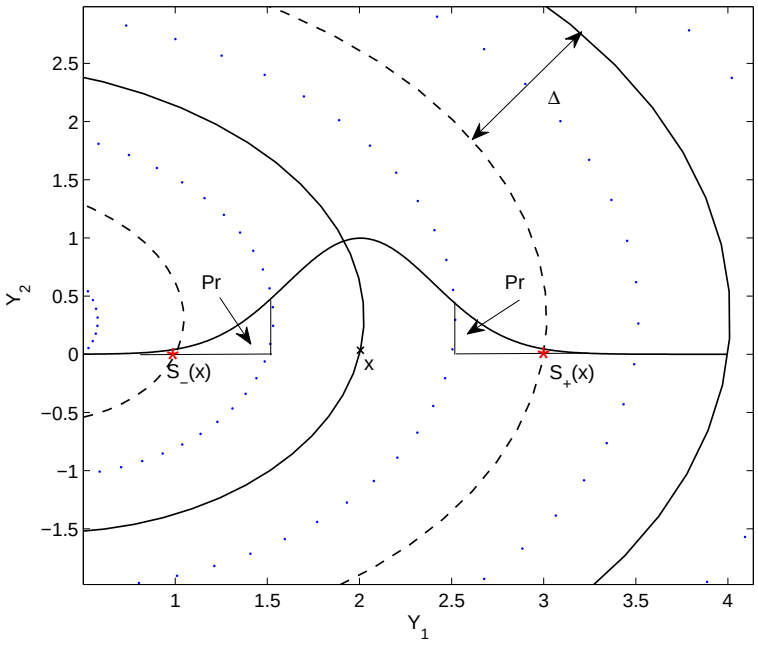

Figure 2.11: Threshold distortion calculation. The dotted curve represents the decision spiral and Pr is the probability of a threshold distortion to occur.

convenient to do the calculations in polar coordinates

$$\begin{aligned} s_+(x) &= s(x) + \Delta \\ -\frac{\Delta}{\pi}(\varphi(\alpha \hat{x}_+)) &= \frac{\Delta}{\pi}(\varphi(\alpha x)) + \Delta. \end{aligned} \tag{2.25}$$

Hence, the reconstructed values can be expressed as follows

$$\hat{x}_\pm = -\eta\Delta\left(\sqrt{\frac{x}{\eta\Delta}} \pm \frac{\pi}{\sqrt{\alpha}}\right)^2 \tag{2.26}$$

where $\eta = 0.16$. For a Gaussian source X, the threshold distortion $\bar{\varepsilon}^2_{\text{th}}$, and the gain

factor α can be expressed, respectively, as follows

$$\begin{aligned}\bar{\varepsilon}_{\text{th}}^2 &\approx \left[1-\text{erf}\left(\frac{\Delta}{2\sqrt{2}\sigma_W}\right)\right]\left[\left(\frac{\pi^4\eta^2\Delta^2}{\alpha^2}+4\sigma_X^2\right)\text{erf}(a)\right. \\ &\quad \left.-\left(\frac{2\pi^2\eta\Delta+a\sigma_X\alpha}{\sqrt{2\pi}\alpha}\right)8\sigma_X e^{-\frac{a^2}{2\sigma_X^2}}+\frac{16\pi^2\eta\Delta\sigma_X}{\sqrt{2\pi}\alpha}\right] \qquad (2.27)\\ \alpha &= \frac{P\eta\sqrt{2\pi^5}}{\Delta\sigma_X(1-e^{-\frac{a}{2\sigma_X^2}})} \qquad (2.28)\end{aligned}$$

where $a = 4\sigma_X$. Fig. 2.12 shows the calculated and the simulated distortion for a $1:2$ spiral mapping under ML decoding. One can notice that the calculated end-to-end distortion $D = \bar{\varepsilon}_{\text{wn}}^2 + \bar{\varepsilon}_{\text{th}}^2$ matches with the simulated MSE $E[(X-\hat{X})^2]$ for moderate to high CSNRs; however, for low CSNRs, there is some mismatch. This shows that (2.21) and (2.27) are very accurate for high CSNR levels. Note that the calculation of the threshold distortion assume that the distance between the spiral arms are equidistant. However, this is not the case close to the origin of the spiral. This makes the calculation to be inaccurate close to the origin and its effect will be prominent at low CSNR levels. This explains in part the mismatch between the two curves in Fig. 2.12 for low CSNRs.

Since it is hard to find an analytical expression for the weak noise and threshold distortion under MAP and MMSE decoding, the optimization of Δ is done numerically by searching for the value of Δ that maximizes the SDR. We create a set of 10^5 source samples $\{x\}$. Knowing the optimized radial distance under ML decoding Δ_{ML}, we form an interval $v = [\Delta_{\text{ML}}/2 \;\; 3\Delta_{\text{ML}}/2]$ in order to choose the radial distance $\Delta \in v$ that gives the best performance. For a given noise variance level, a set of noise samples $\{w\}$ is created to model the AWGN channel. Using MMSE/MAP decoder, we estimate the source sample $\hat{x}$ and evaluate the SDR over the data set $\{x\}$. We

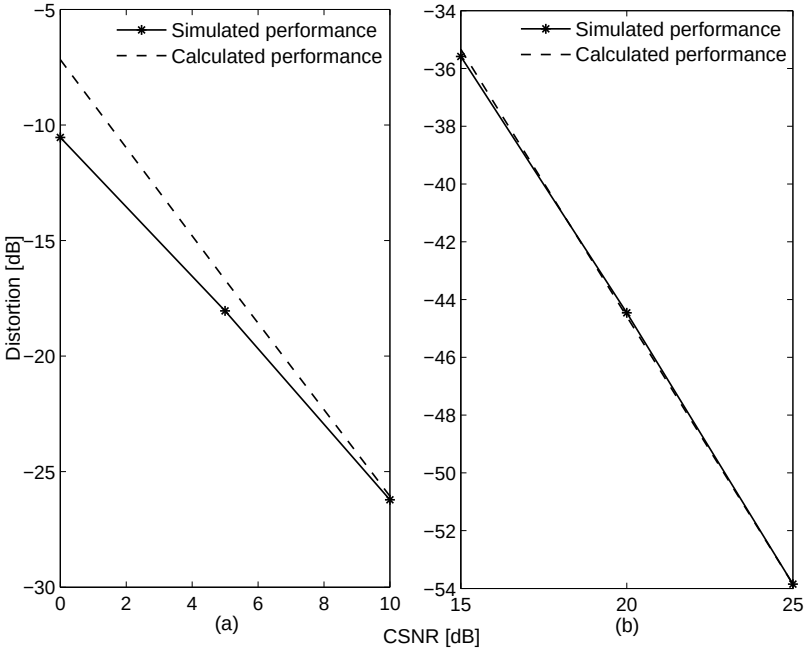

Figure 2.12: Comparison between calculated and simulated performance of $1:2$ spiral mapping under ML decoding. The graph is made for a Gaussian source with standard deviation $\sigma_X = 0.25$.

search over the interval v and choose a Δ that maximizes the SDR. For comparison, we also simulate the system using the Δ optimized for ML decoding (i.e., using (2.20)) but with the MMSE and MAP decoders.

2.4.3 Numerical Results

In this section, we assume an i.i.d. Gaussian source X with standard deviation $\sigma_X = 0.25$. For ML decoding, the radial distance Δ is calculated using (2.20), whereas for MMSE and MAP decoding, numerical search is used to find the Δ value that gives the best performance as described in Section 2.4.2. Comparing Figs. 2.13 and 2.14,

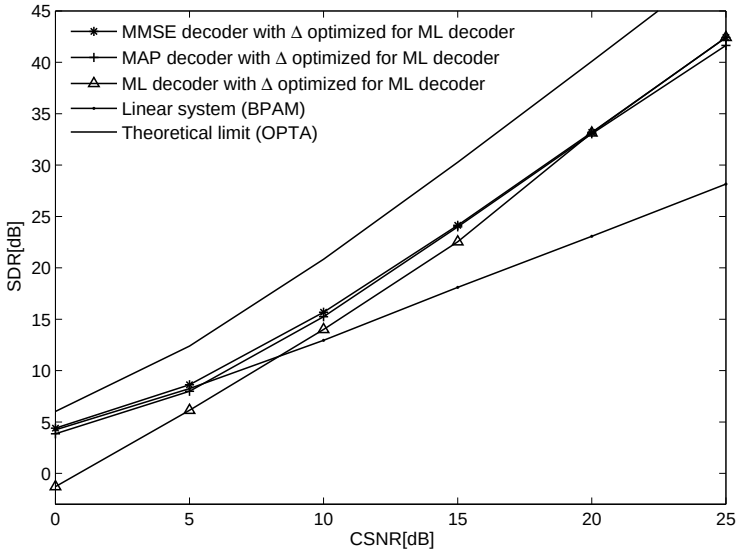

Figure 2.13: Performance of 1:2 bandwidth expansion using spiral mapping. In addition to ML decoder, MMSE and MAP decoders are used at the receiver side. The radial distance Δ is found using (2.20). The optimal linear system (BPAM) and the theoretical limit (OPTA) of the system are also plotted. The graph is made for a Gaussian source X with standard deviation $\sigma_X = 0.25$.

we can notice that MMSE and MAP decoders give better performance than the ML decoder (as expected). There is a substantial improvement at low CSNR levels and the performance from the spiral mapping is now similar to the linear system which is proven to achieve OPTA for asymptotically bad channels [2]. However as CSNR gets large, the ML decoder gives a similar performance as the MMSE decoder. This was expected since the ML decoder approaches that of the optimal decoder in the MSE sense for high CSNR levels [27, pp. 291-292]. When using the optimized Δ for the given decoding technique, we notice around 0.3 dB gain for most CSNR range. The highest gain from optimizing Δ was noticed for the MAP decoder at CSNR = 25 dB; by comparing Figs. 2.13 and 2.14, a 1 dB gain can be noticed from using the

optimized Δ under MAP decoding over the one found using (2.20). However, it is important to mention that for most CSNR range, when using the MMSE or MAP decoders, parameter optimization is less critical and it suffices to use the optimized Δ under ML decoder as given in (2.20).

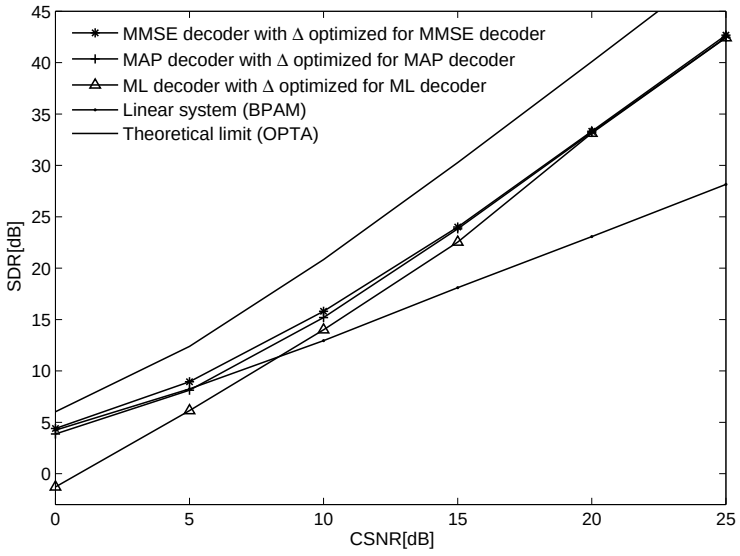

Figure 2.14: Performance of 1:2 bandwidth expansion using spiral mapping. In addition to ML decoder, MMSE and MAP decoders are used at the receiver side. The radial distance Δ is found using the numerical optimization method for MAP and MMSE decoder. The optimal linear system (BPAM) and the theoretical limit (OPTA) of the system are also plotted. The graph is made for a Gaussian source X with standard deviation $\sigma_X = 0.25$.

Motivated by the broadcast scenario, we optimize the encoder for a fixed-design CSNR level and assume that the true CSNR is known at the receiver so that the decoder can be updated accordingly. Figs. 2.15, 2.16, 2.17, and 2.18 show the robustness curve for a design CSNR = 6 and 16 dB. We can observe a large gain from using MMSE and MAP decoding over ML at low CSNRs. Note that ML decoding does not

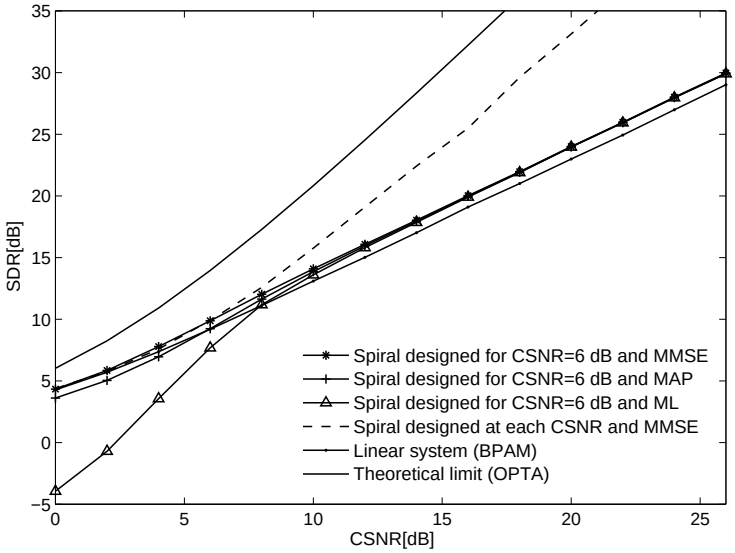

Figure 2.15: Robustness curve for the 1:2 spiral mapping system against a noise mismatch. The receiver side is assumed to know the true CSNR while the encoder is designed for a given CSNR level. The designed CSNR is 6 dB. The performance of a linear system and the OPTA are also shown.

use the knowledge of channel noise in estimating the source symbol. However, both MMSE and MAP decoding use source and channel knowledge to improve the system performance. When the true CSNR is higher than the designed one, the performance is still increasing with a strictly positive slope (slope = 1) which is due to the analog nature of our system; the slope, however, is noticeably less than that of the OPTA curve (slope = 2). This is contrasted with the leveling-off effect (slope = 0) of a purely digital system. However, when the true CSNR is lower than the designed one, the performance decreases drastically especially for ML decoder. This behavior is due to the threshold distortion which happens for bad channel conditions. When using MMSE or MAP, in addition to the noise characteristics, the decoder will use the source knowledge to pick the spiral arm that is more probable to occur. This will lower

the effect of threshold distortion over ML decoding. It is evident that when using MMSE or MAP decoder, the system exhibits various degrees of robustness against mismatch in noise level. More specifically, for low to moderate design CSNR level, the degradation in performance is small when the actual CSNR is lower than the designed one. However, for high design CSNR, we can notice substantial degradation from best performance when the actual CSNR deviates from the designed one. Moreover, when the actual CSNR is higher than the designed one, the performance is increasing with a strictly positive slope. Finally, MMSE decoding incurs less degradation than MAP decoding.

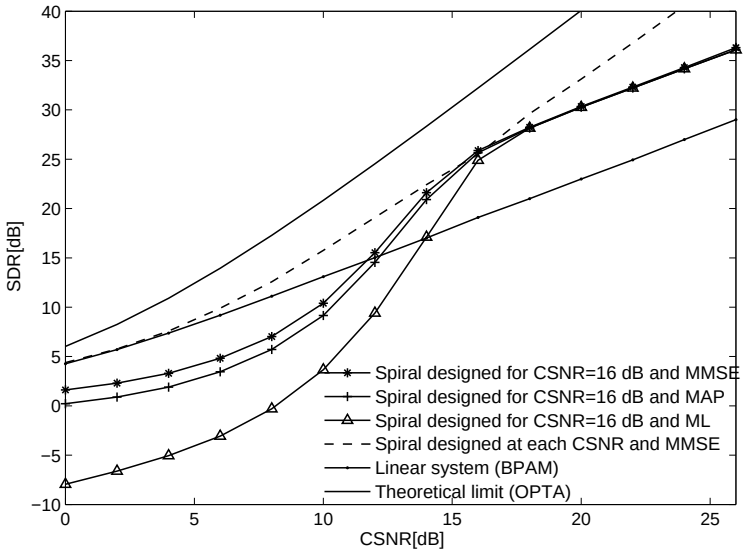

Figure 2.16: Robustness curve for the 1:2 spiral mapping system against a noise mismatch. The receiver side is assumed to know the true CSNR while the encoder is designed for a given CSNR level. The designed CSNR is 16 dB. The performance of a linear system and the OPTA are also shown.

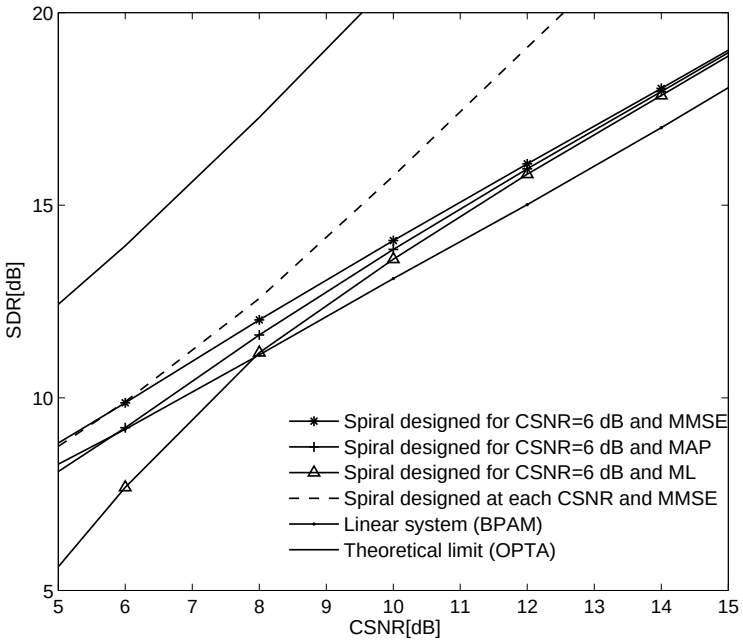

Figure 2.17: A zoomed plot of Fig. 2.15.

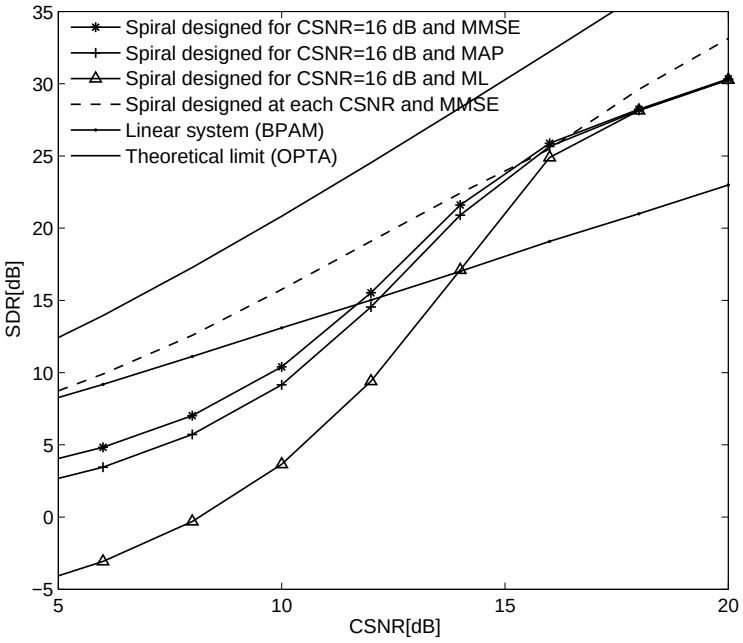

Figure 2.18: A zoomed plot of Fig. 2.16.

Chapter 3

Hybrid Digital-Analog Coding for High Bandwidth Expansion

3.1 Introduction

With the increasing popularity of wireless sensors networks, reliable transmission with delay and complexity constraints is more relevant than ever. A sensor node communicates its sensed field information to a fusion center over a noisy wireless channel. In this chapter, we focus on low delay and low complexity lossy JSCC by proposing a bandwidth expansion scheme based on combining scalar quantizers with a $1:2$ nonlinear analog coder operating on the quantization error. The hybrid scheme HSQLC provides a dimension expansion of rate $r = 2$ [25]. This scheme uses pulse amplitude modulation to send a scalar quantizer output on one channel, and linear uncoded analog transmission of the quantization error on another channel. For rates larger than two ($r > 2$), Coward suggested to repeatedly quantize the error from the

previous quantization step and finish the last step with a linear coder [29]. Recently, a similar system, referred to as "generalized HSQLC", was studied in [30], and shown to achieve the optimal scaling exponent. Our system is closely related to the generalized HSQLC; one main difference is that we are using a non-linear coder in the analog part. Similar hybrid systems based on splitting the source into a quantization part and a quantization error part were also proposed in [22]. These schemes, however, use long channel block codes for the quantization part, thus incurring large delay and complexity and making them not comparable with our proposed low delay/complexity scheme. The rest of the chapter is organized as follows. Section 3.2 describes the system model and optimization for a $1:3$ bandwidth expansion. In Section 3.3, a lower bound on the system SDR is derived. A generalization of the system to account for higher expansion ratio and its performance in the CSNR limit are presented in Section 3.4. Simulation results are included in Section 3.5. Finally, conclusions are drawn in Section 3.6.

3.2 System Model

3.2.1 System Structure

In this section, we assume a memoryless Gaussian source X with variance σ_X^2 to be transmitted over a power limited, discrete time, and continuous amplitude channel with additive white Gaussian noise $W \sim \mathcal{N}(0, \sigma_W^2)$. We propose a $1:3$ bandwidth expansion system that consists of a scalar quantizer and a $1:2$ dimension expansion using Archimedes' spiral, as shown in Fig. 3.1. The proposed system works as follows. A source symbol X is first quantized using an l-level quantizer $\mathrm{Q}(.)$. The quantizer

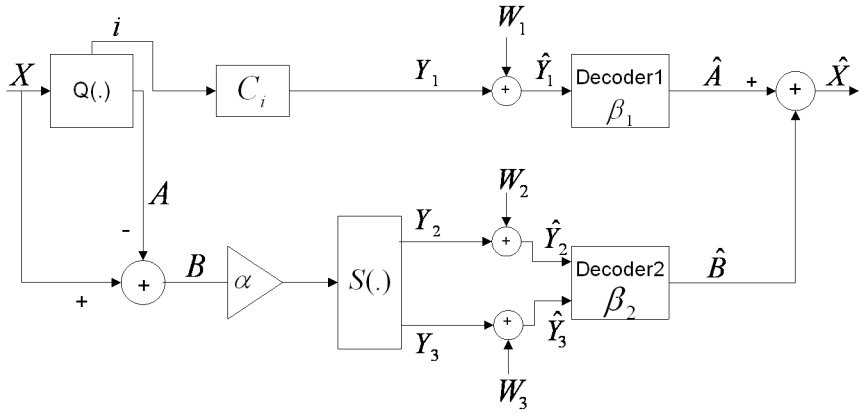

Figure 3.1: System Model.

uses a set of decision intervals $D_i = (d_i, d_{i+1})$ with $d_0 = -\infty$ and $d_l = +\infty$. It returns both the index i and the representation level $A = a_i$, $i = \{0, \ldots, l-1\}$. The index i is represented by the channel input $Y_1 = c_i$. The quantization error $B = X - A$ is mapped to a two-dimensional channel symbol using the 1:2 Archimedes' spiral. The system is optimized to minimize the MSE $\mathbb{E}[(X - \hat{X})^2]$ distortion while satisfying the average channel power constraint P

$$\frac{1}{3}\left\{\mathbb{E}[Y_1^2] + \int ||\mathbf{s}(\alpha b)||^2 f_B(b) db\right\} \leq P \tag{3.1}$$

where α is the gain factor, $f_B(b)$ is the pdf of the quantization error B, and $\mathbf{s}(.)$ denotes the spiral mapping given by

$$\mathbf{s}(b) = \begin{bmatrix} z_1(b) \\ z_2(b) \end{bmatrix} = \frac{1}{\pi} \begin{bmatrix} sgn(b)\Delta\varphi(b)\cos\varphi(b) \\ sgn(b)\Delta\varphi(b)\sin\varphi(b) \end{bmatrix} \tag{3.2}$$

where $sgn(\cdot)$ is the signum function, Δ is the radial distance between any two neighboring spiral arms, and $\varphi(b) = \sqrt{6.25|b|/\Delta}$ [17]. The optimal decoder is

$\beta(\hat{y}_1, \hat{y}_2, \hat{y}_3) \triangleq \mathbb{E}[X|\hat{y}_1, \hat{y}_2, \hat{y}_3] = \mathbb{E}[A|\hat{y}_1, \hat{y}_2, \hat{y}_3] + \mathbb{E}[B|\hat{y}_1, \hat{y}_2, \hat{y}_3]$, where each expectation terms are respectively given as follows

$$
\begin{aligned}
\mathbb{E}[A|\hat{y}_1, \hat{y}_2, \hat{y}_3] &= \frac{\sum_{i=0}^{l-1} a_i f_W(\hat{y}_1 - c_i) \int_{d_i - a_i}^{d_{i+1}-a_i} f_X(b + a_i) f_W(\hat{y}_2 - z_1(\alpha b))}{\sum_{i=0}^{l-1} f_W(\hat{y}_1 - c_i) \int_{d_i - a_i}^{d_{i+1}-a_i} f_X(b + a_i) f_W(\hat{y}_2 - z_1(\alpha b))} \\
&\quad \frac{f_W(\hat{y}_3 - z_2(\alpha b))db}{f_W(\hat{y}_3 - z_2(\alpha b))db} \\
&= \frac{\sum_i a_i e^{-\frac{(\hat{y}_1 - c_i)^2}{2\sigma_W^2}} \int_{d_i - a_i}^{d_{i+1}-a_i} e^{-\frac{(b+a_i)^2}{2\sigma_X^2} - \frac{(\hat{y}_2 - y_1(\alpha b))^2 + (\hat{y}_3 - z_2(\alpha b))^2}{2\sigma_W^2}} db}{\sum_i e^{-\frac{(\hat{y}_1 - c_i)^2}{2\sigma_W^2}} \int_{d_i - a_i}^{d_{i+1}-a_i} e^{-\frac{(b+a_i)^2}{2\sigma_X^2} - \frac{(\hat{y}_2 - z_1(\alpha b))^2 + (\hat{y}_3 - z_2(\alpha b))^2}{2\sigma_W^2}} db} \\
\mathbb{E}[B|\hat{y}_1, \hat{y}_2, \hat{y}_3] &= \frac{\sum_{i=0}^{l-1} f_W(\hat{y}_1 - c_i) \int_{d_i - a_i}^{d_{i+1}-a_i} b f_X(b + a_i) f_W(\hat{y}_2 - z_1(\alpha b))}{\sum_{i=0}^{l-1} f_W(\hat{y}_1 - c_i) \int_{d_i - a_i}^{d_{i+1}-a_i} f_X(b + a_i) f_W(\hat{y}_2 - z_1(\alpha b))} \\
&\quad \frac{f_W(\hat{y}_3 - z_2(\alpha b))db}{f_W(\hat{y}_3 - z_2(\alpha b))db} \\
&= \frac{\sum_i e^{-\frac{(\hat{y}_1 - c_i)^2}{2\sigma_W^2}} \int_{d_i - a_i}^{d_{i+1}-a_i} b e^{-\frac{(b+a_i)^2}{2\sigma_X^2} - \frac{(\hat{y}_2 - z_1(\alpha b))^2 + (\hat{y}_3 - z_2(\alpha b))^2}{2\sigma_W^2}} db}{\sum_i e^{-\frac{(\hat{y}_1 - c_i)^2}{2\sigma_W^2}} \int_{d_i - a_i}^{d_{i+1}-a_i} e^{-\frac{(b+a_i)^2}{2\sigma_X^2} - \frac{(\hat{y}_2 - z_1(\alpha b))^2 + (\hat{y}_3 - z_2(\alpha b))^2}{2\sigma_W^2}} db}
\end{aligned}
\tag{3.3}
$$

with $f_W(.)$ and $f_X(.)$ denote, respectively, the pdf of the Gaussian noise and the source, $\{z_1(\alpha b), z_2(\alpha b)\}$ represents the mapped spiral point as given in (3.2), and $0 \leq i \leq l-1$. Unfortunately, using the optimal joint decoder makes it hard to find a closed form expression for the overall MSE distortion and will certainly increase the system complexity. Since one of our main objectives is to present a simple system for hybrid digital-analog coding with minimized MSE distortion, we will not use the optimal joint decoder. Instead, we use two separate optimal decoders for both the received quantized symbol and the received quantization error. The MMSE decoder

introduced in Section 2.4 is used for recovering the quantization error

$$\beta_2(\hat{y}_2, \hat{y}_3) = \mathbb{E}[B|\hat{y}_2, \hat{y}_3] = \int b f_{B|\hat{Y}_2,\hat{Y}_3}(b|\hat{y}_2, \hat{y}_3)db = \frac{\int b f_{\hat{Y}_2,\hat{Y}_3|B}(\hat{y}_2, \hat{y}_3|b) f_B(b)db}{\int f_{\hat{Y}_2,\hat{Y}_3|B}(\hat{y}_2, \hat{y}_3|b) f_B(b)db} \quad (3.4)$$

where $f_{\hat{Y}_2,\hat{Y}_3|B}(\hat{y}_2, \hat{y}_3|b) = f_W(\hat{y}_2 - z_1(\alpha b)) f_W(\hat{y}_3 - z_2(\alpha b))$. The quantized symbol is decoded using the MMSE estimator as follows

$$\beta_1(\hat{y}_1) = \mathbb{E}[A|\hat{y}_1] = \frac{\sum_{i=0}^{l-1} a_i P(a_i) e^{-\frac{(\hat{y}_1 - c_i)^2}{2\sigma_W^2}}}{\sum_{i=0}^{l-1} P(a_i) e^{-\frac{(\hat{y}_1 - c_i)^2}{2\sigma_W^2}}} \quad (3.5)$$

where $P(a_i) = P(X \in D_i)$ is the probability that $A = a_i$. Note that table-lookup can be used on both decoders to reduce the complexity. We also use a mid-tread uniform quantizer, so that only spacing between levels need to be specified

$$\begin{aligned} a_i &= \big(i - (l-1)/2\big)\delta_a \\ c_i &= K a_i \quad \text{for } \ i \in 0, ..., l-1 \\ d_j &= \big(j - l/2\big)\delta_d \quad \text{for } \ j \in 1, ..., l-1 \end{aligned} \quad (3.6)$$

where δ_a, δ_d represent, respectively, the reproduction and decision levels step, K is a gain factor related to power constraint on Y_1, and the number of quantization level l is assumed to be an odd integer. The distribution of the quantization error B is given by

$$f_B(b) = \sum_{i=0}^{l-1} f_{A,B}(a_i, b) \quad (3.7)$$

where $f_{A,B}(a_i, b)$ can be expressed as follows

$$f_{A,B}(a_i, b) = \begin{cases} f_X(b + a_i), & b \in (d_i - a_i, d_{i+1} - a_i) \\ 0, & \text{Otherwise} \end{cases} . \tag{3.8}$$

Using (3.7), the average channel power constraint in (3.1) becomes

$$\frac{1}{3}\left\{\sigma_{Y_1}^2 + \frac{\alpha\Delta}{\pi^2\eta}\sum_{i=0}^{l-1}\left(\int_{d_i}^{d_{i+1}} |x - a_i| f_X(x)dx\right)\right\} \leq P \tag{3.9}$$

where $\sigma_{Y_1}^2$ is the variance of the channel input Y_1 given by

$$\sigma_{Y_1}^2 = \sum_{i=0}^{l-1} c_i^2 P(X \in D_i) = K\sum_{i=0}^{l-1} a_i^2 \int_{d_i}^{d_{i+1}} f_X(x)dx. \tag{3.10}$$

3.2.2 System Optimization

In this section, we will optimize a target distortion $\text{MSE}_{\text{target}}$

$$\text{MSE}_{\text{target}} = \text{MSE}_{\text{q}} + \text{MSE}_{\text{exp}} \tag{3.11}$$

where MSE_{q} is the distortion in decoding A, and MSE_{exp} is the distortion in decoding B. [1]

[1]Note that $\text{MSE}_{\text{target}}$ is equal to the overall MSE distortion $\mathbb{E}[(X - \hat{X})^2]$ if we were using a centroid quantizer. Moreover, simulations have shown that the difference between the target and the real distortion is very small.

The MSE_{q} is calculated as follows

$$\begin{aligned} \text{MSE}_{\text{q}} &= \mathbb{E}[(A-\hat{A})^2] = \mathbb{E}[(A-\beta_1(C(A)+W))^2] \\ &= \int_{-\infty}^{+\infty} \sum_{i=0}^{l-1} (a_i - \beta_1(c_i+w))^2 P(a_i) f_W(w) dw. \end{aligned} \tag{3.12}$$

The distortion from the spiral mapping MSE_{exp} is given by

$$\text{MSE}_{\text{exp}} = \mathbb{E}[(B-\hat{B})^2] \approx \bar{\varepsilon}^2_{\text{wn}} + \bar{\varepsilon}^2_{\text{th}} \tag{3.13}$$

where the weak noise $\bar{\varepsilon}^2_{\text{wn}}$ is given by

$$\bar{\varepsilon}^2_{\text{wn}} \approx \frac{\sigma_W^2}{\alpha^2} \tag{3.14}$$

and the threshold distortion $\bar{\varepsilon}^2_{\text{th}}$ is calculated by inserting (3.7) into (2.23)

$$\begin{aligned} \bar{\varepsilon}^2_{\text{th}} \approx\ & 8\left[1-\text{erf}\left(\frac{\Delta}{2\sqrt{2}\sigma_W}\right)\right]\left[\frac{\sigma_X^2}{2} + \frac{\eta^2\Delta^2\pi^4}{8\alpha^2} + \sum_{i=0}^{l-1}\left(\frac{a_i^2}{2}\right.\right. \\ & \left.\left. -\frac{\pi^2\eta\Delta}{\alpha}a_i\right)\int_{d_i}^{d_{i+1}} f_X(x)dx - a_i\int_{d_i}^{d_{i+1}} x f_X(x)dx\right]. \end{aligned} \tag{3.15}$$

Note that (3.14) and (3.15) are calculated assuming ML decoder; hence, they are very accurate for representing system distortion under MMSE decoding at high CSNR levels.

We minimize the target distortion $\text{MSE}_{\text{target}}$ with respect to the quantizer parameters (δ_d, δ_a, K) in (3.6), and to the spiral parameters (Δ,α). For a given amount of power P_1 assigned to channel input Y_1 (i.e., $\sigma^2_{Y_1} = P_1$), the quantizer parameters (δ_d, δ_a) are

found by minimizing the target distortion $\text{MSE}_{\text{target}}$ in (3.11). The gain factor K is used to control the power allocation on Y_1 and is found from the power constraint P_1 using (3.10). The spiral parameters (Δ, α), which affect only the analog part of the system, are calculated by minimizing (3.13) under the power constraint in (3.9). The optimization of the quantizer parameters is performed over a range of (δ_d, δ_a) values to obtain the one that produces the minimum MSE_{target} distortion. The design algorithm is formally stated as follows.

1. Choose some initial values for (δ_d, δ_a, l).
2. Set $i = 0$, the target distortion $D^{(0)} = \infty$, $D_{\text{best}} = \infty$, and the power assigned to Y_1, $P_1 = \beta P$, $0 \leq \beta \leq 3$.
3. Set $i \leftarrow i + 1$, and find K according to (3.10).
4. For the given quantizer parameters, find the optimal spiral parameters (Δ, α) that minimize (3.13) while (3.9) is satisfied with equality.
5. Calculate MSE_{q} using (3.12), and $D^{(i)}$ using (3.11).
6. If $D_{\text{best}} > D^{(i)}$, set $D_{\text{best}} \leftarrow D^{(i)}$, and $R \leftarrow (\delta_d, \delta_a, K, \Delta, \alpha, D_{\text{best}}, P_1)$.
7. Loop over the quantizer parameters (δ_d, δ_a) values until we reach the end of the range limits, and go to Step 3.
8. Return R.

In our simulations, we used $l = 35$, $\beta = 1$ (i.e., the power constraint at the quantized symbol is equal to the average power constraint P).

3.3 System Lower Bound on the SDR

In this section, we derive a lower bound on the proposed system SDR following the approach of [30]. For this bound, we assume (suboptimal) ML decoding for recovering both the quantized symbol and quantization error.

For the quantized symbol, the system works as follows. At the encoder side, the quantized symbol is scaled by a gain factor K to satisfy the power constraint and transmitted through the channel. At the receiver, the channel output is rescaled using $1/K$, and a ML decoder, which is a minimum distance estimator, is applied on the rescaled signal $\hat{Y}_1 = A + \tilde{W}$, where $\tilde{W} \sim \mathcal{N}(0, (\frac{\sigma_W}{K})^2)$. The error in decoding the quantized value can be expressed as follows

$$\begin{aligned} \mathbb{E}[(A-\hat{A})^2] &= \delta_a^2 \sum_{i=0}^{l-1} P(a_i) \sum_{j=0}^{l-1} (j-i)^2 P_{i,j} \\ &\leq \delta_a^2 l \sum_{g=1}^{l-1} g^2 P_g \end{aligned} \tag{3.16}$$

where $g = |j-i|$, and $P_g = P_{i,j}$ is the probability of receiving a_j when a_i is transmitted, given by

$$P_{i,j} = Q\left(\frac{(|j-i|-1/2)\delta_a}{\frac{\sigma_W}{K}}\right) - Q\left(\frac{(|j-i|+1/2)\delta_a}{\frac{\sigma_W}{K}}\right) \tag{3.17}$$

where $j = 2, ..., l-2$, and $Q(x)$ is the Gaussian Q-function which can be upper bounded for $x \geq 0$ as

$$Q(x) = \frac{1}{\sqrt{2\pi}} \int_x^\infty e^{-\tau^2/2} d\tau \leq \frac{1}{2} e^{-x^2/2}. \tag{3.18}$$

Using (3.18) and dropping the second term in (3.17), the transition probability $P_{i,j}$

can be upper bounded by

$$P_{i,j} \leq \frac{1}{2} \exp\left(-K^2 \frac{(g-1/2)^2 \delta_a^2}{2\sigma_W^2}\right). \tag{3.19}$$

Thus (3.16) can be expressed as follows

$$\begin{aligned} \mathbb{E}[(A-\hat{A})^2] &\leq \frac{\delta_a^2 l}{2} \sum_{g=1}^{l-1} g^2 \exp\left(-\frac{(K\delta_a)^2 (g-1/2)^2}{2\sigma_W^2}\right) \\ &\leq \frac{\delta_a^2 l}{2} \exp\left(-\frac{K^2\delta_a^2}{8\sigma_W^2}\right) \\ &\quad + \frac{\delta_a^2 l}{2} \sum_{g=2}^{l-1} g^2 \exp\left(-\frac{(K\delta_a)^2 g}{2\sigma_W^2}\right) \end{aligned} \tag{3.20}$$

where we have used the fact that $(g-1/2)^2 > g$ for $g \geq 2$. The summation can be bounded to obtain an upper bound on the distortion from decoding the quantized symbol

$$\begin{aligned} \sum_{g=2}^{\ell} g^2 z^g &\leq \sum_{g=1}^{\ell} g^2 z^g = \frac{z}{(1-z)^3}\big(1 + z - (\ell+1)^2 z^\ell \\ &\quad + (2\ell^2 + 2\ell - 1) z^{\ell+1} - \ell^2 z^{\ell+2}\big) \end{aligned} \tag{3.21}$$

where $z = \exp\left(-\frac{(K\delta_a)^2}{2\sigma_W^2}\right)$, and $\ell = l - 1$.

The distortion from decoding B is bounded by

$$\mathbb{E}[(B-\hat{B})^2] \leq \bar{\varepsilon}_{\text{wn}}^2 + \bar{\varepsilon}_{\text{th}}^2 \tag{3.22}$$

where $\bar{\varepsilon}_{\text{wn}}^2$ and $\bar{\varepsilon}_{\text{th}}^2$ are, respectively, the weak noise and threshold distortion (under ML decoding) given by (3.14) and (3.15). Adding (3.20) and (3.22) gives an upper

bound on the end-to-end distortion, thus yielding a lower bound on the system SDR.

3.4 Asymptotic Achievable Scaling Exponent

For a memoryless Gaussian source with variance σ_X^2 and AWGN noise with power σ_W^2, the average MSE distortion D and the average transmission power P are related by the converse lossy joint source-channel coding theorem as

$$R(D) \leq rC(P) \tag{3.23}$$

where $R(D) = 0.5\log(\sigma_X^2/D)$, $D < \sigma_X^2$, is the rate-distortion function, $C(P) = 0.5\log(1+P/\sigma_W^2)$ is the capacity function of the channel, and $r = m$ is the expansion ratio for $1 : m$ bandwidth expansion system. Therefore, (3.23) can be expressed as follows

$$\text{SDR} \leq (1+\text{CSNR})^m. \tag{3.24}$$

The optimal scaling exponent as CSNR goes to infinity is defined as $\lim_{\text{CSNR}\to\infty}(\ln \text{SDR} / \ln \text{CSNR}) = m$ [30]. In this section, we focus on the system behavior as CSNR goes to infinity and we generalize the system to achieve higher expansion ratio using the multiple stage quantizer as proposed in [29] and recently in [30]. This is done by coding the source symbol using multiple stages of quantizers and finishing with a 1:2 nonlinear analog encoder at the last stage. To encode a single source sample X into

$m \geq 3$ channel symbols $Y_1, ..., Y_m$, we proceed by first finding the pairs (A_i, B_i), via

$$\begin{aligned} A_i &= (\delta_a)^i \text{int}\left(\frac{B_{i-1}}{(\delta_a)^i}\right) \\ B_i &= (B_{i-1} - A_i) \end{aligned} \tag{3.25}$$

where $i = 1, ..., m-2$, $B_0 = X$, δ_a is the quantization resolution, and $\text{int}(\theta)$ is the unique integer j such that $\theta \in [j - \frac{1}{2}, j + \frac{1}{2})$. Note that A_i represents the hierarchical quantization of the source, and B_i is the associated quantization error.

Proposition 1 *[30] As δ_a goes to zero, the variance of A_i converges to that of B_{i-1}, $i = 1, ..., m-2$.*

Proposition 2 *As δ_a goes to zero, the quantization error B_i is uniformly distributed on the interval $[-(\delta_a)^i/2, (\delta_a)^i/2]$.*

The A_i's and B_i's satisfy the following properties

1. The mapping $X \to (A_1, ..., A_{m-2}, B_{m-2})$ is one-to-one and

$$X = \sum_{i=1}^{m-2} A_i + B_{m-2}. \tag{3.26}$$

2. The variance of B_0 is σ_X^2, and B_i has a variance approximately (for sufficiently small δ_a) equal to $(\delta_a)^{2i}/12$, for $i = 1, ..., m-2$. This follows directly from Proposition 2.

3. The variance of the A_i's are given by

$$\sigma_{A_i}^2 \approx \begin{cases} \sigma_X^2, & \text{for } i = 1 \\ \delta_a^{2(i-1)}/12, & \text{for } i = 2, ..., m-2 \end{cases}. \tag{3.27}$$

This directly follows from Propositions 1 and 2.

To complete the description of the transmission strategy, A_i's are scaled by $K_i = \sqrt{P/\sigma_{A_i}^2}$ to satisfy the power constraint, and B_{m-2} is mapped to a two-dimensional space using the Archimedes's spiral as in (3.2). The weak noise $\bar{\varepsilon}_{\text{wn}}^2$ can be written as in (2.21), where the gain factor α is calculated in a similar way to (2.22)

$$\alpha = \frac{8\pi^2\eta P}{\Delta(\delta_a)^{m-2}}. \tag{3.28}$$

From the assumption that the quantization error follows a uniform distribution (for sufficiently small δ_a), the threshold distortion $\bar{\varepsilon}_{\text{th}}^2$ can be expressed using (2.23) as follows

$$\bar{\varepsilon}_{\text{th}}^2 \approx \left[1 - \text{erf}\left(\frac{\Delta}{2\sqrt{2}\sigma_W}\right)\right]\left[\frac{8p^3}{3} + \frac{8\pi^2\eta\Delta p^2}{\alpha} + \frac{2\pi^4\eta^2\Delta^2 p}{\alpha^2}\right] \tag{3.29}$$

where $p = (\delta_a)^{m-2}/2$. To study the system behavior when CSNR goes to $+\infty$, we assume (suboptimal) ML decoding, which is a minimum distance estimator, for recovering the quantized symbols and the quantization error. Note that ML decoding approaches that of the optimum estimate in the MSE sense as CSNR gets large [27, pp. 291-292].

The overall MSE $\mathbb{E}[(X-\hat{X})^2]$ distortion under MMSE decoding can upper bounded by the distortion from decoding A_i's and B_{m-2}, via

$$\text{MSE} \leq \sum_{i=1}^{m-2} \mathbb{E}[(A_i - \hat{A}_i)^2] + \mathbb{E}[(B_{m-2} - \hat{B}_{m-2})^2] \tag{3.30}$$

where $\hat{A}_i$'s and $\hat{B}_{m-2}$ are, respectively, the estimated quantized symbols and quantization error from ML decoder. At the receiver, the received quantized symbol is rescaled by $1/K_i$ and the ML decoder is used. The error in decoding the received quantized symbols can be calculated in a similar approach to (3.20). Using the fact that the first term in (3.20) will dominate the summation when $l \to \infty$ and for large values of $(\delta_a)^2(\text{CSNR})$, the distortion in decoding the quantized symbols can be upper bounded by

$$\mathbb{E}[(A_i - \hat{A}_i)^2] \leq c(\delta_a)^{2i} \exp\left(-\kappa(\delta_a)^2(\text{CSNR})\right) \tag{3.31}$$

where c and κ are some positive constants, and $i = 1, ..., m-2$.

The distortion in decoding the quantization error $\mathbb{E}[(B_{m-2} - \hat{B}_{m-2})^2]$ is given by

$$\mathbb{E}[(B_{m-2} - \hat{B}_{m-2})^2] \leq \bar{\varepsilon}^2_{\text{wn}} + \bar{\varepsilon}^2_{\text{th}} \tag{3.32}$$

where the weak noise $\bar{\varepsilon}^2_{\text{wn}}$ and threshold distortion $\bar{\varepsilon}^2_{\text{th}}$ are given by (2.21) and (3.29), respectively. The optimized radial distance Δ is observed numerically to fit well the following function

$$\Delta = \sqrt{P} a \exp\left(-b\text{CSNR}_{\text{dB}}\right) \tag{3.33}$$

where a and b are some positive constant. Using (3.33) in (2.21), and (3.29), the weak and threshold distortion can be expressed as follows

$$\begin{aligned}\bar{\varepsilon}^2_{\text{wn}} &\approx \frac{a^2(\delta_a)^{2(m-2)}}{64\pi^4\eta^2\text{CSNR}^{\left(1+\frac{20b}{\ln 10}\right)}} \\ \bar{\varepsilon}^2_{\text{th}} &\approx (\delta_a)^{3(m-2)}\left[1-\text{erf}\left(\frac{a\text{CSNR}^{\left(\frac{1}{2}-\frac{10b}{\ln 10}\right)}}{2\sqrt{2}}\right)\right] \\ &\quad \left[\frac{1}{3}+\frac{a^2\text{CSNR}^{\left(-\frac{20b}{\ln 10}\right)}}{4}+\frac{a^4\text{CSNR}^{\left(-\frac{40b}{\ln 10}\right)}}{64}\right].\end{aligned} \tag{3.34}$$

Using the bound on the Gaussian Q-function as given in (3.18), the threshold distortion can be upper bounded by

$$\begin{aligned}\bar{\varepsilon}^2_{\text{th}} &\leq \left[(\delta_a)^{3(m-2)}\exp\left(-\frac{a^2\text{CSNR}^{\left(1-\frac{20b}{\ln 10}\right)}}{8}\right)\right] \\ &\quad \left[\frac{1}{3}+\frac{a^2\text{CSNR}^{\left(-\frac{20b}{\ln 10}\right)}}{4}+\frac{a^4\text{CSNR}^{\left(-\frac{40b}{\ln 10}\right)}}{64}\right].\end{aligned} \tag{3.35}$$

When $(\delta_a^2\text{CSNR})$ goes to infinity, the quantization error in (3.31) decreases exponentially. This happens for increasing CSNR if we set $\delta_a^2 = \text{CSNR}^{(\epsilon-1)}$, for some $\epsilon > 0$. Taking $b = \frac{\ln 10}{20} - \epsilon^{'}$, where $\epsilon^{'} > 0$, the threshold distortion decreases exponentially, and the weak noise can be expressed as follows

$$\bar{\varepsilon}^2_{\text{wn}} \approx \frac{a^2(\text{CSNR})^{(\epsilon-1)(m-2)}}{64\pi^2\eta^2\text{CSNR}^{\left(2-\frac{20}{\ln 10}\epsilon^{'}\right)}}. \tag{3.36}$$

Hence the overall distortion, which will be dominated by the weak noise, satisfies

$$\mathbb{E}[(X-\hat{X})^2] \in O\left(\mathrm{CSNR}^{-(m-\epsilon^{''})}\right) \tag{3.37}$$

where $\epsilon^{''} = (m-2)\epsilon + \frac{20}{\ln 10}\epsilon^{'}$.[2] Therefore, the scaling exponent for a fixed ϵ and $\epsilon^{'}$ is

$$\begin{aligned} \lim_{\mathrm{CSNR}\to\infty} \frac{\ln \mathrm{SDR}}{\ln \mathrm{CSNR}} &\geq \lim_{\mathrm{CSNR}\to\infty} \frac{\ln \sigma_X^2 + (m-\epsilon^{''})\ln \mathrm{CSNR}}{\ln \mathrm{CSNR}} \\ &= m-\epsilon^{''}. \end{aligned} \tag{3.38}$$

Note that ϵ and $\epsilon^{'}$ represent a tradeoff, i.e., for a small ϵ the error due to the quantized part vanishes slowly, but the scaling exponent in the limit is larger; and for a small $\epsilon^{'}$ the threshold distortion vanishes slowly whereas the scaling exponent gets larger in the limit.

3.5 Numerical Results

In this section, we again assume an i.i.d. Gaussian source X with variance $\sigma_X^2 = 1$. We simulate a $1:3$ bandwidth expansion system as described in Section 3.2. As reference systems, we consider 1) the optimal linear system ($1:3$ BPAM) which is the best possible linear solution [2], and 2) a $1:3$ HDA-Linear system which differs from the proposed system by using a $1:2$ linear coder on the quantization error. This system was optimized to achieve the best possible performance. As shown in Fig. 3.2, the proposed system has the highest performance over all CSNR levels. Moreover, the performance of the HDA-Linear and BPAM system approach that of the proposed

[2]The "Big-O" notation is defined as follows. Let $f(x)$ and $g(x)$ be two functions on $\mathbb{R}$. We write $f(x) \in O(g(x))$ if and only if for all $x \geq x_0$ we have $f(x) \leq cg(x)$, where c is some constant.

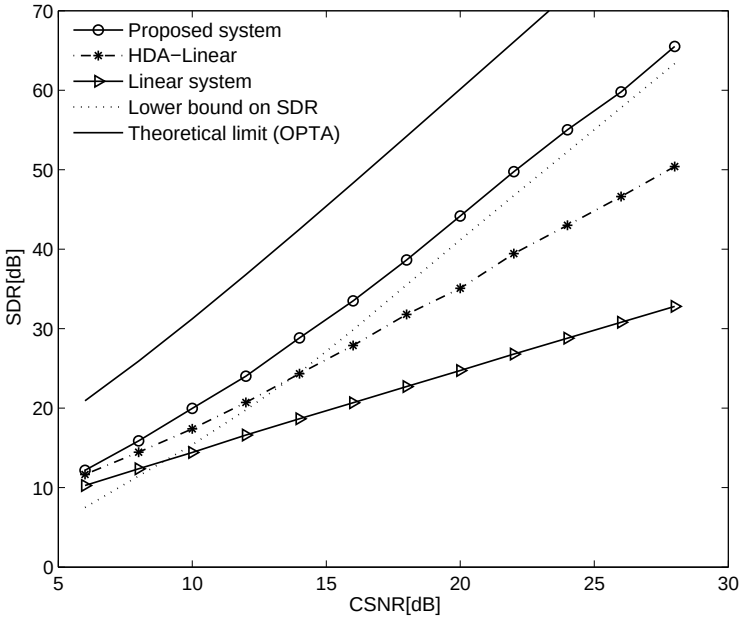

Figure 3.2: Performance of the proposed system for $X \sim \mathcal{N}(0,1)$. This system is also compared to the HDA-Linear, the optimal linear system (BPAM) [2], and OPTA. The lower bound on system SDR is also plotted.

one at low CSNRs. Comparing our system to the $1:3$ PCCOVQ found in [14], we can notice that both systems have similar performance for CSNR$\leq$ 15 dB. However, as the CSNR gets large, the computational complexity from the design algorithm of the PCCOVQ gets too large and make it intractable to design the system [14]. Hence, the main advantage of our system over the PCCOVQ is in the design complexity. The lower bound on the proposed system SDR, derived in Section 3.3, is also shown in Fig. 3.2. Notice that the lower bound is a good approximation for moderate to high CSNRs and is a few dBs away from the actual performance at low CSNRs. It is important to note that the theoretical limit is achieved asymptotically using infinite-size block code in the source and the channel coders. Hence, the gap between the

theoretical limit and our low-delay system is not surprising.

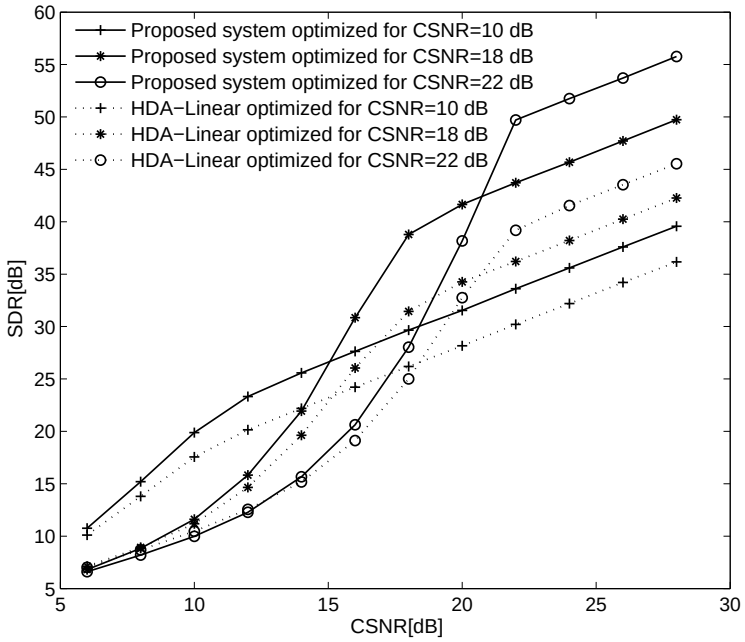

Figure 3.3: The robustness curves for the proposed (solid line) and the HDA-Linear (dotted line) system against a noise mismatch. The graph is made for a unitary Gaussian source.

Motivated by the broadcast scenario, we also optimize the encoder for a fixed-design CSNR level and assume that the true CSNR is known at the receiver so that the decoder can be updated accordingly. The solid and the dotted curves in Fig. 3.3 represent, respectively, the performance of the proposed and the HDA-Linear system when there is a mismatch between the design and the true CSNR level. It is evident that both systems exhibit various degrees of robustness against mismatch in noise level. The gap between the proposed and the reference system increases as CSNR gets large; at low CSNRs, we can notice that both system achieve similar performance. Fig. 3.3 suggests that a system that provides a given SDR level at a lower CSNR level

is less sensitive to mismatch than one that is less sensitive to mismatch than one that achieves the same SDR at a higher CSNR level. Fig. 3.4 shows the channel space structure optimized for CSNR = 20 dB. The solid line represents neighbors in the one-dimensional source space. Note that the channel space is discontinuous due to the use of scalar quantization.

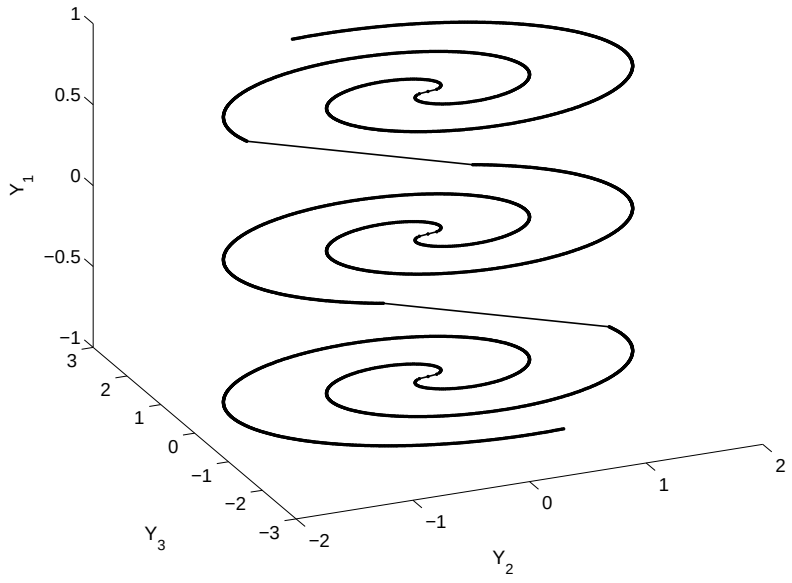

Figure 3.4: Channel signal set for a $1:3$ bandwidth expansion designed for CSNR = 20 dB. Each point on this mapping corresponds to a specific $\mathbf{Y} = (Y_1, Y_2, Y_3)$. The lines drawn between the selected $\mathbf{Y}$ show the correspondence between neighbors in the one dimensional reconstructed signal. The lines linking the spiral end points represent the jump to another quantized point.

3.6 Summary and Conclusion

In this chapter, we have presented a low-delay lossy joint source-channel coding scheme which combines scalar quantizers and a $1:2$ nonlinear analog coder. The proposed system is evaluated and optimized numerically to minimize the MSE given an average channel power constraint for a $1:3$ bandwidth expansion. Simulation results have shown that the proposed system outperforms both purely linear analog system and the $1:3$ HDA-Linear due to the use of a nonlinear analog coder on the quantization error. Also, our system has shown to achieve similar performance as the $1:3$ PCCOVQ system. However, the advantage in our system is the low design complexity which is very high in the other system. Moreover, the hybrid scheme, which has low complexity and low delay, has been generalized to achieve higher expansion ratios. This is done by coding the source symbol using multiple stages of quantizers and finishing with a 1:2 nonlinear analog encoder at the last stage. This communication strategy has shown to achieve a near optimal scaling exponent in the CSNR limit.

Chapter 4

Analog Source-Channel Coding for Low Bandwidth Expansion

4.1 Introduction

In the previous chapter, we studied a lossy source-channel coding system with bandwidth expansion ratio M/N, where M is an integer≥ 3 and $N = 1$. In this chapter, we present a system with a (fractional) bandwidth expansion ratio of $1 < M/N < 2$. This scheme is based on the combination of a $1:1$ uncoded system in which each symbol is scaled to its power constraint and a $1:2$ bandwidth expansion system in which each source symbol is mapped to a two-dimensional channel input for protection over noisy channels. This combination makes any overall expansion ratio between 1:1 and 1:2 achievable. In other words, this is a $N:M$ bandwidth expansion system as long as the condition $N < M < 2N$ is fulfilled. Power is optimally allocated between $1:1$ uncoded and $1:2$ nonlinear systems in order to maximize the overall performance.

In [31] a system that gives an overall compression ratio between 2 : 1 and 1 : 1 is proposed based on the combination of 1 : 1 and 2 : 1 systems. The rest of the chapter is organized as follows. Section 4.2 presents the problem considered and develops the system model. In Section 4.3, we introduce the power allocation strategy. Simulation results are included in Section 4.4. Finally, conclusions are drawn in Section 4.5.

4.2 System Model

We again consider a memoryless Gaussian source X with variance σ_X^2 for transmission over the AWGN channel with noise variance σ_W^2 (i.e., $W \sim \mathcal{N}(0, \sigma_W^2)$). Samples from the source X are grouped into blocks of size N denoted by $\mathbf{X}^N$. Depending on the overall expansion ratio, the source vector $\mathbf{X}^N$ is split into two subvectors of dimension L and $N - L$. The L symbols are transmitted using the 1 : 1 uncoded system and the other $N - L$ symbols use 1 : 2 bandwidth expansion system to protect transmission over noisy channels. By properly choosing the subvectors dimensions, any overall expansion ratio between 1 : 1 and 1 : 2 can be achieved. The system, which is shown in Fig. 4.1, includes a power allocator which is responsible for determining how much power is allocated to each subvectors. Note that this system can be seen as a group of sensors that has the ability to either use uncoded transmission or 1 : 2 bandwidth expansion. In what follows, we will briefly describe both uncoded and expansion systems.

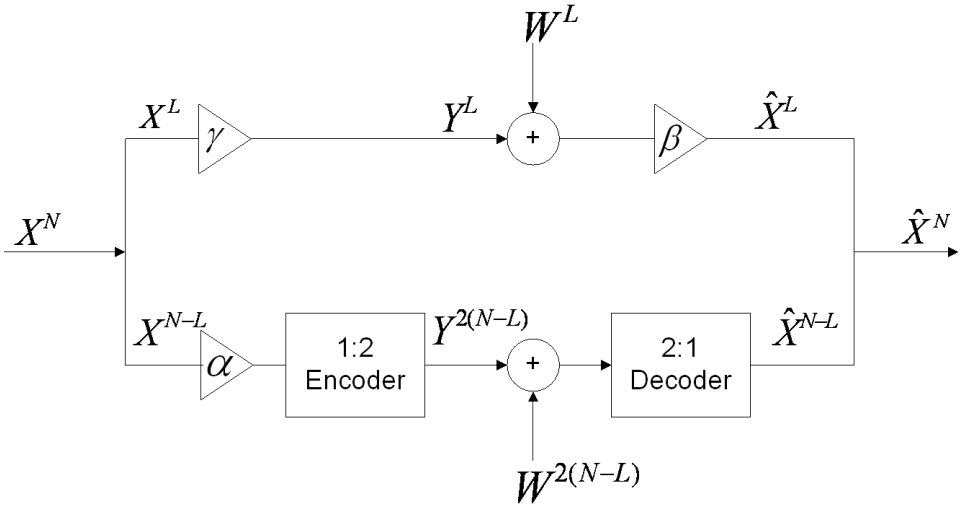

Figure 4.1: Proposed system where L and $N-L$ symbols are transmitted using $1:1$ and $1:2$ system, respectively.

4.2.1 1:1 Uncoded System

It is known that for the case of memoryless Gaussian source X over AWGN channel with matched bandwidth, uncoded, or linear, transmission is optimal [32]. This system is obtained by simply using the transmitter

$$Y = \gamma X = \frac{\sigma_Y}{\sigma_X} X \tag{4.1}$$

and the receiver

$$\hat{X} = \beta \hat{Y} = \frac{\gamma \sigma_X^2}{\gamma^2 \sigma_X^2 + \sigma_W^2} \hat{Y} \tag{4.2}$$

where σ_Y^2 is the average channel power constraint, and $\hat{Y}$ is the noisy received signal. This gives an MSE equal to

$$D_{\text{uncoded}} = \mathbf{E}[(X - \hat{X})^2] = \sigma_X^2 \left(1 + \frac{\sigma_Y^2}{\sigma_W^2}\right)^{-1}. \tag{4.3}$$

Comparing (4.3) to the distortion from OPTA, it is clear that the 1 : 1 uncoded system achieves the theoretical limit.

4.2.2 1:2 Bandwidth Expansion

In order to perform 1 : 2 bandwidth expansion, we use the double Archimedes' spiral in a similar fashion to Section 2.4. At the receiver side, we use the optimal MMSE decoder instead of ML decoder used in [17]. Under ML decoding, the overall distortion from using spiral mapping can be expressed as follows [17]

$$D_{\text{ML}} = \bar{\varepsilon}_{\text{wn}}^2 + \bar{\varepsilon}_{\text{th}}^2 \tag{4.4}$$

where $\bar{\varepsilon}_{\text{wn}}^2$ and $\bar{\varepsilon}_{\text{th}}^2$ are the weak noise and threshold distortion, respectively. Hence, the calculated performance of the 1 : 2 spiral mapping under ML decoding is SDR $= \sigma_X^2/(\bar{\varepsilon}_{\text{wn}}^2 + \bar{\varepsilon}_{\text{th}}^2)$.

As shown in Fig. 4.2, it can be noticed that the performance of the 1 : 2 spiral mapping with MMSE decoder is close to the calculated performance of the optimal linear system (BPAM) at low CSNRs (≤ 10) dB, and to the 1 : 2 bandwidth expansion system with ML decoding at high CSNRs (≥ 10) dB. Since it is hard to find an analytical expression for the system performance under MMSE decoding, we use the

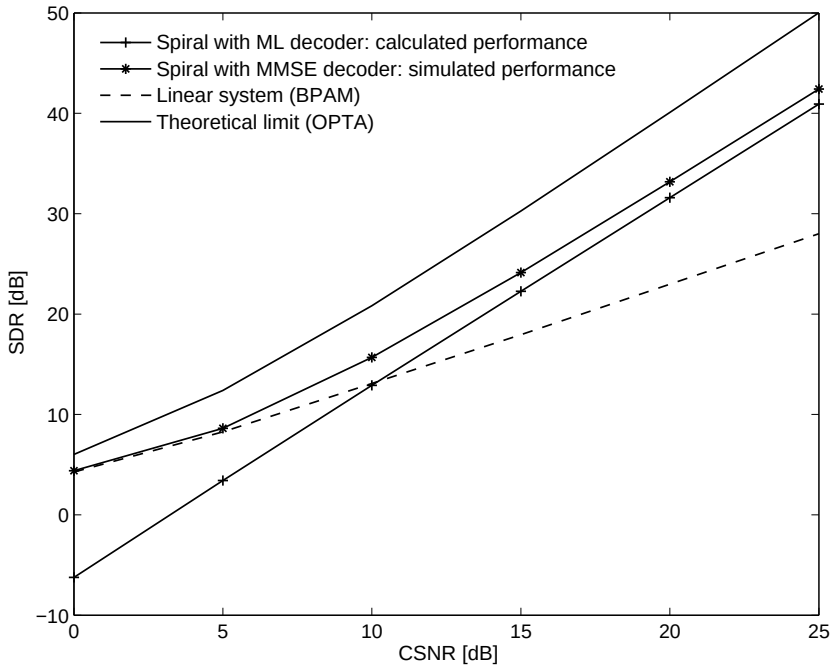

Figure 4.2: Performance of the 1:2 bandwidth expansion system for a Gaussian source with standard deviation $\sigma_X = 0.25$. The graph showns the simulated performance under MMSE decoder and the calculated performance under ML decoder. The performance of a linear system and the OPTA are also plotted.

following approximation

$$D_{\text{exp}} \approx \begin{cases} D_{\text{BPAM}} = \left(\frac{\sigma_X \sigma_W}{\sigma^2_{Y_2}+\sigma^2_W}\right)^2 \left(\sigma^2_W + \frac{\sigma^4_{Y_2}}{2}\right), & 0 \leq \text{CSNR} \leq 10\text{dB} \\ D_{\text{ML}} \approx \bar{\varepsilon}^2_{\text{wn}} + \bar{\varepsilon}^2_{\text{th}}, & \text{otherwise} \end{cases} \tag{4.5}$$

where $\sigma^2_{Y_2}$ is the average power constraint on the channel input, D_{BPAM} and D_{ML} are, respectively, the distortion from the $1:2$ BPAM and $1:2$ spiral expansion under ML decoding. In Fig. 4.2, this is given by the dashed curve for $0 \leq$CSNR≤ 10 dB and by the solid curve (with pluses) for CSNR> 10 dB.

4.3 Optimal Power Allocation

Without loss of generality, we assume that the average power constraint per channel use is set to 1. The total power allocated for both $1:1$ uncoded transmission and $1:2$ expansion system is $L+2(N-L)$. Denoting by $p \in (0,1)$ the proportion of the total power allocated for the uncoded system, then the power for transmitting each channel symbol is $\sigma_Y^2 = \frac{(L+2(N-L))p}{L}$ in the $1:1$ system and $\sigma_{Y_2}^2 = \frac{(L+2(N-L))(1-p)}{2(N-L)}$ in the $1:2$ system. Thus γ in Fig. 4.1 can be found as follows

$$\gamma = \frac{\sigma_Y}{\sigma_X} = \frac{\sqrt{\frac{(L+2(N-L))p}{L}}}{\sigma_X}. \tag{4.6}$$

The gain factor α is related to the average power constraint in the $1:2$ system $\sigma_{Y_2}^2$, via

$$\sigma_{Y_2}^2 = \frac{1}{2}\int ||\mathbf{s}(\alpha x)||^2 f_X(x)dx \tag{4.7}$$

where $f_X(x)$ is the source pdf, and $\mathbf{s}(.)$ denotes the $1:2$ spiral mapping described in chapter 2. For a Gaussian source, α can be expressed as follows

$$\alpha = \frac{\sigma_{Y_2}^2 \eta \sqrt{2\pi^5}}{\Delta \sigma_X (1 - e^{-\frac{a^2}{2\sigma_X^2}})} \tag{4.8}$$

where $\eta = 0.16$, Δ is the radial distance of the spiral mapping, and $a = 4\sigma_X$.

The average MSE distortion $\bar{D} \triangleq \mathbb{E}[(\mathbf{X}^N - \hat{\mathbf{X}}^N)^2]/N$ is given by

$$\bar{D} = \frac{\mathbb{E}[(\mathbf{X}^L - \hat{\mathbf{X}}^L)^2] + \mathbb{E}[(\mathbf{X}^{N-L} - \hat{\mathbf{X}}^{N-L})^2]}{N} = \frac{LD_{\text{uncoded}} + (N-L)D_{\text{exp}}}{N} \tag{4.9}$$

where D_{uncoded} and D_{exp} are given in (4.3) and (4.5), respectively.

Given L, $(N-L)$ (i.e. expansion rate), and a noise level σ_W^2, $\bar{D}$ can be expressed as a function of p. Thus, it is possible to find numerically the optimal power allocation p by solving the following unconstraint optimization problem

$$p_{opt} = \arg\min_p \bar{D} = \arg\min_p (LD_{\text{uncoded}} + (N-L)D_{\text{exp}}). \tag{4.10}$$

Fig. 4.3 shows the average power allocation in the $1:2$ nonlinear system for different

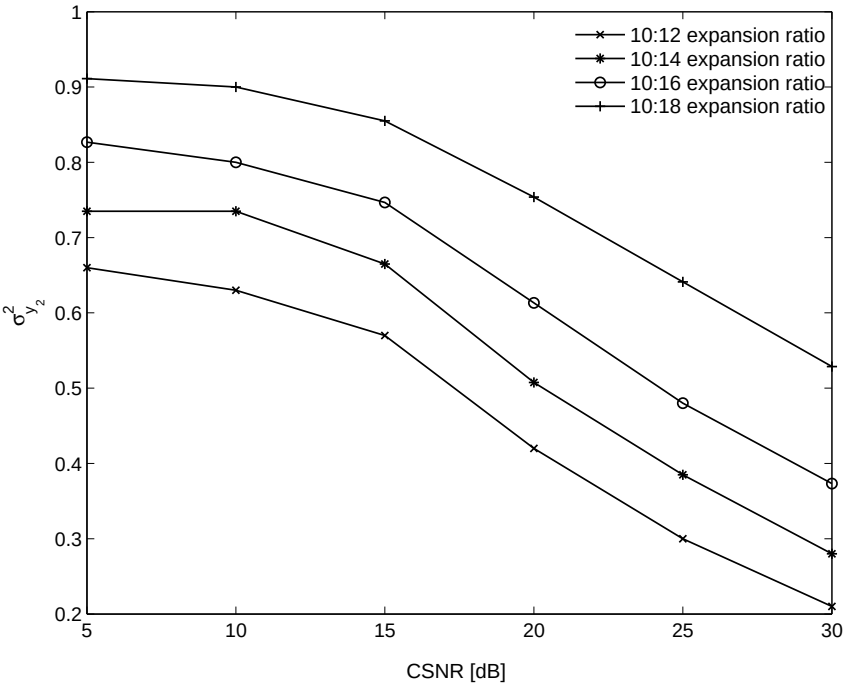

Figure 4.3: Average power allocated for each channel symbol in the 1:2 nonlinear system. The plot is made for a Gaussian source with standard deviation $\sigma_X = 0.25$.

expansion ratio as a function of CSNR level. For a given expansion ratio, one can notice that the average channel power allocated for the 1:2 system decreases as CSNR increases. This can be explained by the fact that the difference in output SDR between

1 : 1 and 1 : 2 system increases with CSNR which requires more power to be allocated to the 1 : 1 uncoded system. Notice also that the average channel power allocated to the 1 : 2 system is less than 1, which is the average channel power for the whole system. This means that the average power per channel use in the 1 : 1 system is higher than in the 1 : 2 nonlinear system. This can be explained by the fact that the distortion from the 1 : 1 system is always greater than the distortion from 1 : 2 system; hence more power should be allocated to the 1 : 1 system in order to balance the distortion from both uncoded and bandwidth expansion system to decrease the overall distortion.

4.4 Numerical Results

In this section, we assume a Gaussian source X with standard deviation $\sigma_X = 0.25$ and $N = 10$. In order to show the improvement brought by optimizing the power allocation, we compare the performance of the proposed system when applying optimal power allocation using (4.10) to the system when power is equally allocated to each channel symbol. Figs. 4.4, 4.5, 4.6, and 4.7 show the system performance for expansion ratio 10 : 12, 10 : 14, 10 : 16, and 10 : 18, respectively. The performance of the system when the optimal power allocation is found by numerical search is also plotted. This is done by calculating through simulation the output SDR for different power allocation (p) and choosing the one that give the best performance. This is represented by the dashed curve which shows similar performance when optimizing p using (4.10). For reference, we also compare the proposed scheme to the optimal linear system (BPAM) [2]. From simulation plots, we can notice that the proposed

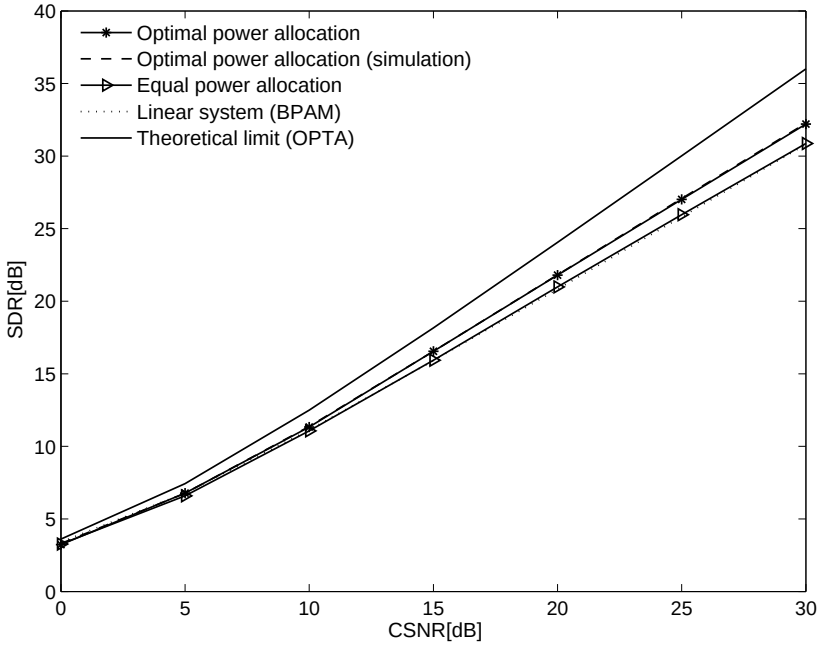

Figure 4.4: Performance of the proposed system for 10:12 expansion ratio for a Gaussian source with standard deviation $\sigma_X = 0.25$ and $N = 10$.

system outperforms the linear system even without power allocation. The gain over the linear system increases as the expansion ratio increases. However, at low CSNR levels, both system gives similar performance. When using power allocator, the system SDR increases by several dB for moderate to high CSNRs over the one without power allocator. This substantial improvement in SDR increases as CSNR and the expansion ratio increase. By comparing the dashed line and the solid line (with asterisk), we can notice that the simulated performance matches with the performance from the theoretical analysis.

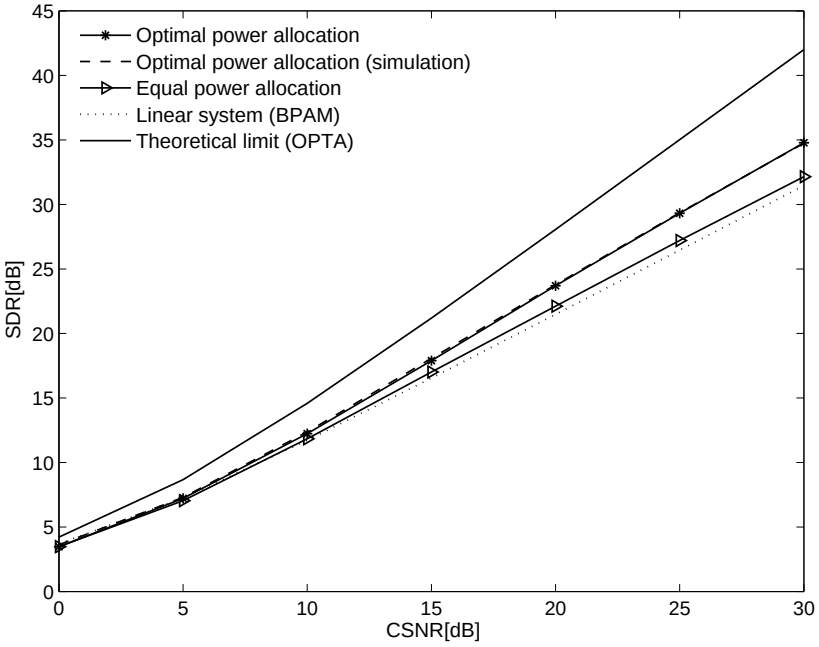

Figure 4.5: Performance of the proposed system for 10:14 expansion ratio for a Gaussian source with standard deviation $\sigma_X = 0.25$ and $N = 10$.

4.5 Summary and Conclusion

In this chapter, we have presented a lossy purely analog joint source-channel coding which combines uncoded transmission and a $1:2$ bandwidth expansion system using the spiral mapping. The proposed system, which is able to achieve any overall expansion ratio between 1 and 2, is evaluated and optimized to minimize the MSE distortion under an average channel power constraint. This is done by allocating power properly between the uncoded and the expansion systems. Simulation results have shown that the proposed scheme outperforms the purely analog linear system. Moreover, using optimal power allocation, the system has shown to give several dB gain over the one without power allocation.

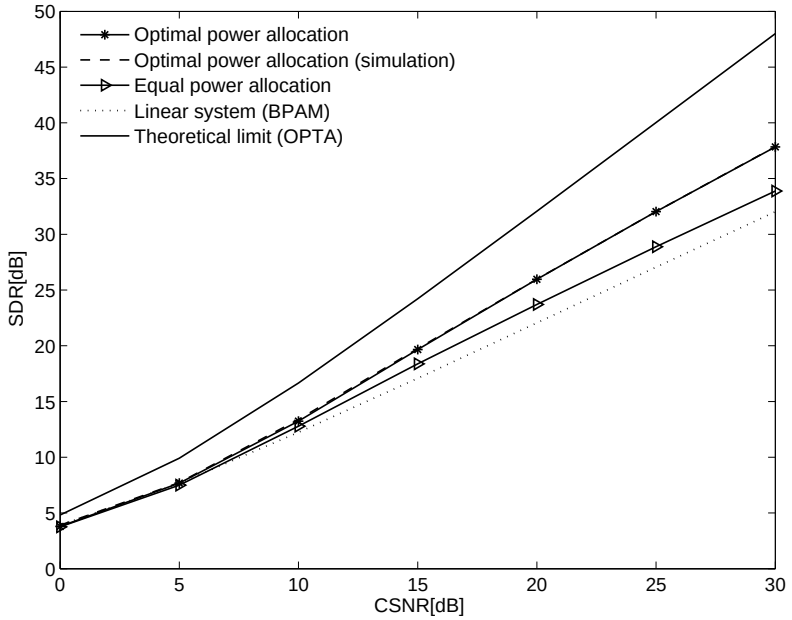

Figure 4.6: Performance of the proposed system for 10:16 expansion ratio for a Gaussian source with standard deviation $\sigma_X = 0.25$ and $N = 10$.

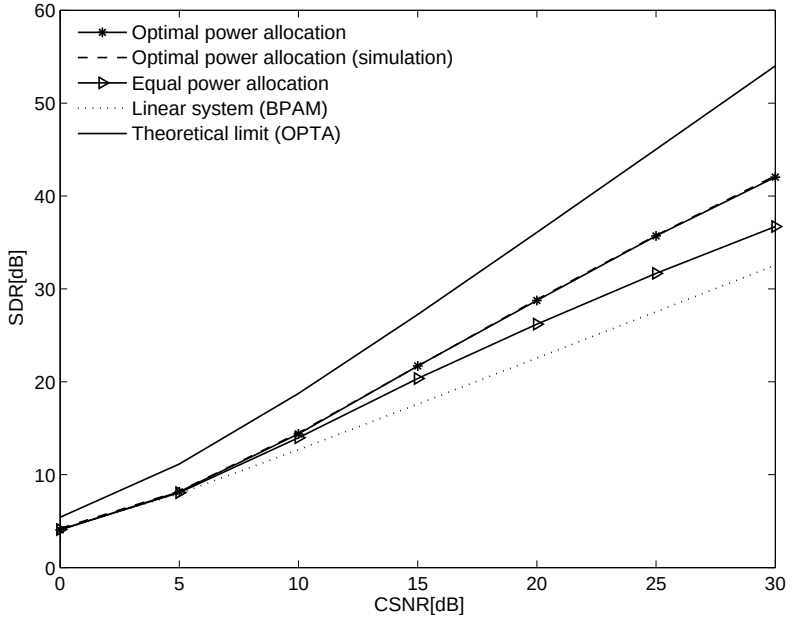

Figure 4.7: Performance of the proposed system for 10:18 expansion ratio for a Gaussian source with standard deviation $\sigma_X = 0.25$ and $N = 10$.

Chapter 5

Compressed Sensing with Shannon-Kotel'nikov Mappings

5.1 Introduction

Wireless sensor networking is a technology that monitors the physical world through a distributed network of wireless sensor nodes. These nodes, often conceived as having limited lifetime and processing power, communicate their sensed field information to a fusion center (FC). Communication takes place over power and bandwidth constrained noisy wireless channels [33]. To meet these challenges, we investigate using low delay/complexity source-channel mapping with compressed sensing in WSNs.

The sensor inputs are treated as samples from an analog source. The traditional approach for analog source transmission is to use separate digital source and channel coders. This separation is optimal from a theoretical perspective [3]. In such systems, the analog source is encoded using a powerful vector quantizer, and capacity

approaching channel codes, such as turbo or low-density-parity-check codes, are used for channel error protection. This approach results in very high delay and complexity, which is not desirable in WSNs. The approach used here is analog joint source-channel coding which has been shown to achieve an excellent performance under low delay and complexity constraints [1, 15, 7, 8, 17, 34]. More specifically, we propose to use $1:2$ Shannon-Kotel'nikov mappings within the CS context. The key idea is to use nonlinear dimension expansion, that acts as an analog joint source-channel encoder on the compressed sensing measurements to increase their immunity against channel noise. In [35], a hybrid digital-analog system is used with distributed compressed sensing over noisy channels. In this Chapter, we consider a purely-analog system where all sensed and transmitted signals are analog-valued. For reference, we compare the proposed system with 1) a conventional CS system that assumes noiseless transmission, and 2) a CS-based system that accounts for channel noise during signal reconstruction [36]. Both reference systems are used with 1:1 linear mapping. The rest of this chapter is organized as follows. In Section 5.2, we briefly review the compressed sensing theory. In Section 5.3, we develop the system structure and its optimization. Simulation results are included in Section 5.4. Finally, conclusions are drawn in Section 5.5.

Note that in this chapter, we will not use a superscript (e.g., $\mathbf{X}^N$) for vectors as opposed to previous chapters. We will simply use bold symbols.

5.2 Overview of Compressed Sensing Theory

The theory of compressed sensing has been developed in [9, 37, 38, 36]. In essence, CS exploits prior knowledge about the sparsity of a signal $\mathbf{x} \in \mathbb{R}^N$ in order to provide efficient signal sampling and reconstruction [36]. The signal $\mathbf{x}$ is assumed to be sparse in some orthonormal basis $\mathbf{\Psi}$

$$\mathbf{x} = \mathbf{\Psi}\mathbf{u} \tag{5.1}$$

where $\mathbf{u}$ is the transform coefficients vector in the orthobasis $\mathbf{\Psi}$. The sparsity assumption means that there is only K ($K \ll N$) nonzero elements in $\mathbf{u}$.

In CS we record $M < N$ linear measurements, which can be expressed as

$$\mathbf{y} = \mathbf{\Phi}\mathbf{x} \tag{5.2}$$

where $\mathbf{\Phi} \in \mathbb{R}^{M \times N}$ is a measurement matrix which obeys the restricted isometry property [39]. This property can be achieved when the entries of the matrix $\mathbf{\Phi}$ are i.i.d. Gaussian variables. In this case, with M in the order of $K \log_2(N/K)$, recovery of $\mathbf{x}$ from the linear measurements $\mathbf{y}$ works with overwhelming probability, and is conducted by solving the following convex optimization problem

$$\min_{\hat{\mathbf{x}}} ||\mathbf{\Psi}^T \hat{\mathbf{x}}||_{\ell_1}, \text{ subject to } \mathbf{\Phi}\hat{\mathbf{x}} = \mathbf{y} \tag{5.3}$$

where $||(\cdot)||_{\ell_1}$ is the ℓ_1 norm ($||\mathbf{x}||_{\ell_1} \triangleq \sum_{i=1}^{N} |x_i|$) and $(.)^T$ denotes the transpose operator. Several optimization algorithms were developed to solve the ℓ_1 minimization problem such as basis pursuit (BP) [10], matching pursuit [11], and orthogonal matching pursuit [40].

In practice, the collected measurements are usually disturbed by noise $\mathbf{w}$; thus $\mathbf{y}$ is modeled as

$$\mathbf{y} = \mathbf{\Phi x} + \mathbf{w}. \tag{5.4}$$

For CS to be widely applicable, signal recovery should be robust against noise; a small disturbance in the measurements should result in a small disturbance in the signal reconstruction. Using a noise-aware version of (5.3), the signal can be reconstructed as follows

$$\min_{\hat{\mathbf{x}}} ||\mathbf{\Psi}^T \hat{\mathbf{x}}||_{\ell_1}, \text{ subject to } ||\mathbf{\Phi}\hat{\mathbf{x}} - \mathbf{y}||_2 \leq \epsilon \tag{5.5}$$

where ϵ bounds the total amount of noise in the measurements. This convex problem can be expressed using the Lagrange multipliers as

$$\min_{\hat{\mathbf{x}}} ||\mathbf{\Psi}^T \hat{\mathbf{x}}||_{\ell_1} + \lambda ||\mathbf{\Phi}\hat{\mathbf{x}} - \mathbf{y}||_2^2. \tag{5.6}$$

This is often referred to as the least absolute shrinkage and selection operator problem [41]. The term λ is used to control the tradeoff between the sparsity and the approximation error ($||\mathbf{\Phi}\hat{\mathbf{x}} - \mathbf{y}||_2$).

5.3 System Model

5.3.1 System Structure

Consider a group of sensors that is observing a discrete time continuous amplitude source signal $\mathbf{x} \in \mathbb{R}^N$. This observation is assumed to be sparse in some transform basis $\mathbf{\Psi}$. Each sensor encodes its observation and transmits it to the FC over additive

white Gaussian noise channels with variance σ_w^2. The objective is to recover the sensor observations under a mean square error fidelity criterion. The proposed system structure is shown in Fig 5.1.

On the encoder side, the sensors measure the observation using a random projection matrix $\mathbf{\Phi}$. A practical method is to draw each entry of the projection matrix independently from a Gaussian distribution (i.e., $[\Phi]_{ij} \sim \mathcal{N}(0, 1/M)$) and then orthogonalize the rows of Φ. The measurement vector is given by

$$\mathbf{y} = \mathbf{\Phi x}, \tag{5.7}$$

where $\mathbf{\Phi} \in \mathbb{R}^{M \times N}$ is the measurement matrix for the CS encoder. Each sample of the measurement vector $\mathbf{y}$ is mapped to a two-dimensional channel space using the double Archimedes' spiral as given in Section 2.4

$$\mathbf{s}(y) = \begin{bmatrix} z_1(y) \\ z_2(y) \end{bmatrix} = \frac{1}{\pi} \begin{bmatrix} sgn(y)\Delta\varphi(y)\cos\varphi(y) \\ sgn(y)\Delta\varphi(y)\sin\varphi(y) \end{bmatrix} \tag{5.8}$$

where $sgn(\cdot)$ is the signum function, Δ is the radial distance between any two neighboring spiral arms, and $\varphi(y) = \sqrt{6.25|y|/\Delta}$. It is observed that the measurements from the CS encoder fit well a Gaussian distribution. Hence, for simplicity, the radial spiral distance Δ is calculated using (2.20), where the weak noise $\bar{\varepsilon}^2_{\text{wn}}$, and the threshold distortion $\bar{\varepsilon}^2_{\text{th}}$ can be found in a similar way to (2.21) and (2.27), respectively.

At the receiver side, we use the MMSE decoder to obtain the measurement estimate $\hat{\mathbf{y}}$. To recover the original signal, we use BP [10] to solve the ℓ_1 minimization problem in (5.3), and for comparison also the minimization in (5.6).

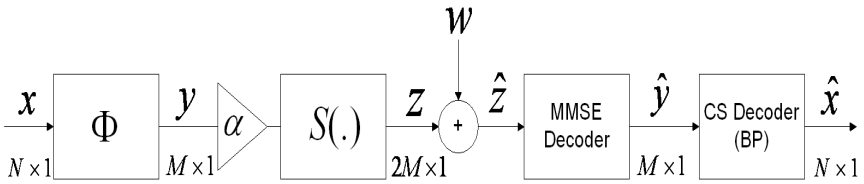

Figure 5.1: The proposed system structure.

5.3.2 System Optimization

The proposed system is optimized for minimal end-to-end MSE distortion $\mathbb{E}[||\mathbf{x}-\hat{\mathbf{x}}||^2]$ which is a function of two sources of distortion: D_{CS} from compressed sensing (without lossy transmission) and D_{exp} from channel noise. Given a total transmission power constraint P_{tot}, the aim is to minimize the end-to-end distortion. From CS theory, it is known that the distortion D_{CS} decreases with increasing number of measurements. However, due to the total power constraint, the average power per channel (use) will decrease. This will increase the distortion D_{exp} from bandwidth expansion transmission. Thus, for a given channel quality, we aim to determine the optimal number of measurements which balances these two distortion contributions and results in a minimum overall distortion under the power constraint P_{tot}.

Distortion D_{exp} from dimension expansion is minimized by optimizing Δ using (2.20). In the CS literature, however, there is not yet an explicit relation between the number of measurements M and the distortion D_{CS} obtained with BP. Thus optimization is done numerically by searching for the number of measurements that minimizes the end-to-end MSE distortion $\mathbb{E}[||\mathbf{x}-\hat{\mathbf{x}}||^2]$. We create a set of source vectors $\{\mathbf{x}\}$ with signal dimension N. Each source vector is synthesized as $\mathbf{x} = \mathbf{\Psi u}$, where $\mathbf{\Psi}$ is the sparsity basis and $\mathbf{u}$ is a K sparse transform coefficients. There are $\binom{N}{K}$ possible

sparsity patterns for $\mathbf{u}$.[1] Each realization is drawn uniformly from these patterns. For each number of measurements M, we create a fixed measurement matrix $\mathbf{\Phi}$ whose entries are drawn from a Gaussian distribution. The set of CS measurement vectors $\{\mathbf{y}\}$ is calculated using (5.7). For a given noise variance level, (Δ, α) are optimized using (2.20) under the average power constraint $P = P_{\text{tot}}/(2M)$, and a set of noise vectors $\{\mathbf{w}\}$ is created to model the AWGN channel. A 1:2 bandwidth expansion is applied on each vector measurements using the Archimedes' spiral in (5.8). Then, the measurement estimate $\hat{\mathbf{y}}$ is decoded using MMSE decoder and BP is used for signal reconstruction according to (5.3). The end-to-end MSE distortion $\mathbb{E}[||\mathbf{x} - \hat{\mathbf{x}}||^2]$ is evaluated over the data set $\{\mathbf{x}\}$. We keep increasing the number of measurements M until we observe an increase in the end-to-end distortion. The design suboptimal search algorithm is shown herein.[2]

In our simulations, we used $T = 30000$, m is set to a small value ($\sim K$), and the incremental step $Inc = 4$.

Fig. 5.2 shows the system SDR as a function of the number of measurements M at different TSNR $\triangleq P_{\text{tot}}/\sigma_w^2$ levels.[3] Notice that for a fixed TSNR level, the SDR increases with increasing M until reaching a maximum and then starts to decrease. This occurs because the compressed sensing part performs better as M increases but at the same time, the distortion from channel noise increases. For small M, the CS distortion dominates over the distortion contributions from channel noise. This is clearly shown from the closeness between the SDR curves as well as from the steep increase in SDR of each curve, which is a trend observed in CS theory. As M gets

[1] The sparsity pattern is the set of the indices of nonzero components of $\mathbf{u}$.

[2] One source of suboptimality is that the system parameters are not jointly optimized to minimize end-to-end distortion.

[3] TSNR stands for "total" SNR and is related to CSNR as TSNR/$(2M)$.

Algorithm 1 System Optimization

Data Input: Input a data set $\mathcal{X} = \{\mathbf{x}_1, \ldots, \mathbf{x}_T\}$, a channel noise variance σ_w^2, and a transmission power constraint P_{tot}.
Initialization: Set the number of measurements $M = m$, the incremental step Inc for the number of measurements, and $i = 1$. Set the end-to-end MSE distortion $D^{(0)} = 10^{20}\text{T}$, $D^{(1)} = 10^{19}\text{T}$, the spiral radial distance $\Delta = \infty$, and the gain factor $\alpha = \infty$.
while $D^{(i)} < D^{(i-1)}$ **do**
$i \leftarrow i + 1$.
Set $\Delta_{\text{opt}} \leftarrow \Delta$, $\alpha_{\text{opt}} \leftarrow \alpha$, and $D_{\text{opt}} \leftarrow D^{(i-1)}$.
Initialize the measurement matrix $\mathbf{\Phi}^{(i)}$ as a random Gaussian matrix.
Obtain measurement vector $\mathbf{y}$ for each observation in $\mathbf{X}$ according to (5.7).
Scale the average channel power constraint according to $P = \frac{P_{\text{tot}}}{2M}$, so that power is equally divided between channels.
Optimize (Δ, α) for the given channel noise variance σ_w^2 according to (2.20) under the power constraint $\mathbb{E}[z^2] = P$.
Map each element in $\mathbf{y}$ to a two-dimensional channel space using (3.2).
Decode $\hat{\mathbf{y}}$ using MMSE decoder according to (3.4), and $\hat{\mathbf{x}}$ using BP according to (5.3).
Calculate numerically $D^{(i)} = \mathbb{E}[||\mathbf{x} - \hat{\mathbf{x}}||^2]$ over the data set $\mathcal{X}$.
$M \leftarrow M + Inc$.
end while
$M \leftarrow M - Inc$.
Return $(M, D_{\text{opt}}, \Delta_{\text{opt}}, \alpha_{\text{opt}})$.

larger beyond a certain level (∼38), the CS distortion contribution levels off, and the trend in the SDR curves follow the performance of the bandwidth expansion systems. We notice around 7 dB gap in system SDR between neighboring curves. For a given M, there is a 4 dB difference in CSNR between adjacent SDR curves. From Fig. 5.2, it can be seen that for M between 40-90, the CSNR levels are in the range 8-19 dB. For a 4 dB difference in CSNR in this range, a $1:2$ bandwidth expansion system using double Archimedes' spiral gives $6 \sim 8$ dB SDR gain [17]. This explains the ~ 7 dB gap between neighboring curves. Thus the trends in Fig. 5.2 show clearly the dominance of CS distortion for small M and channel noise for large M.

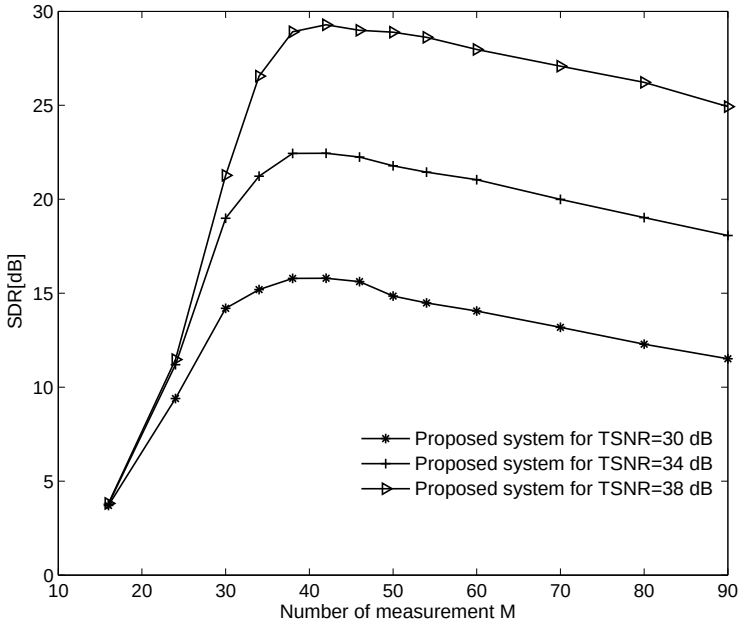

Figure 5.2: Performance of the proposed system as a function of number of measurements M with sparsity level $K = 6$ and signal length $N = 100$. For TSNR=38dB, the CSNR [dB] levels at the data points are as follows: [22.9 21.2 20.2 19.7 19.2 18.7 18.4 18 17.6 17.2 16.5 15.9 15.4]. Note that there is a 4dB difference in CSNR levels (as well as in TSNR) between adjacent curves. MMSE decoding and BP are used on the receiver side.

5.4 Numerical Results

In this section, we assume a sparse source $\mathbf{x}$ in the discrete cosine transform basis $\mathbf{\Psi}$ with signal length $N = 100$. The signal $\mathbf{x}$ is synthetically generated as $\mathbf{\Psi u}$, where there is only $K = 6$ nonzero elements in the transform coefficients $\mathbf{u}$ ($||\mathbf{u}||_{\ell_0} = K \ll N$). The results presented here are for the case where the nonzero elements u_i are i.i.d. Gaussian with unitary variance and the sparsity pattern is uniformly distributed. We use the spiral mapping to apply $1 : 2$ dimension expansion, and BP to recover the

source signal $\hat{\mathbf{x}}$ from the received measurements.

The conventional CS system "CS-BP" which uses BP for signal recovery, does not account for channel noise during reconstruction. However, as mentioned in Section 5.2, there is also a noise-aware version of ℓ_1 minimization in CS theory that can recover source signal from noisy measurements [36]. The structure of these linear analog reference systems is shown in Fig. 5.3. We scale the channel input by a gain factor γ in order to satisfy the average channel power constraint $P = \mathbb{E}[(\gamma y)^2] = \gamma^2 \mathbb{E}[y^2]$. At the receiver, we use a MMSE optimal scaling factor $\beta = \gamma \mathbb{E}[y^2]/(\gamma^2 \mathbb{E}[y^2] + \sigma_w^2)$ to obtain an estimate of $\mathbf{y}$, and use either BP or basis pursuit with denoising (BPDN) [10] for signal reconstruction. This is conducted by solving the optimization problem stated in (5.3) or (5.5).

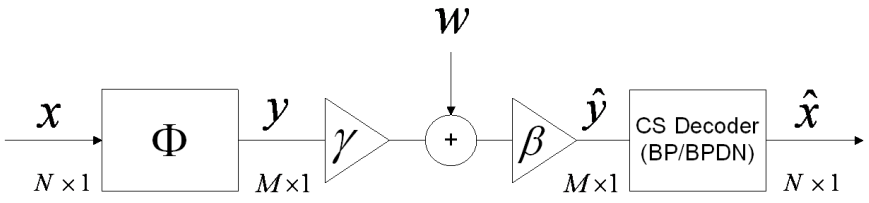

Figure 5.3: CS-BP/CS-BPDN structure with 1:1 linear mapping.

The number of measurements M is optimized for all systems under the total transmission power P_{tot}. This is done using Algorithm 1 for the proposed system, whereas for the reference systems, we search over a range of M to obtain the one that produces the minimum end-to-end distortion. Since the number of measurements varies with the channel noise variance, system SDR is plotted based on TSNR. From Fig. 5.4, it can be seen that the proposed system "CS-Mapping" outperforms the CS-BP system for all CSNR levels, and "CS-BPDN" from moderate to high CSNRs. At low CSNRs,

CS-BPDN gives similar performance as the CS-Mapping. This can be explained by realizing that the 1 : 2 bandwidth expansion using the double Archimedes' spiral has a similar performance as a linear encoder at low CSNR levels [17]. Notice that the gain from CS-Mapping as well as its gap to CS-BPDN gets more prominent as CSNR increases. We also simulate the proposed system when using BPDN instead of BP on the noisy decoded measurement $\hat{\mathbf{y}}$. This gives around 1 dB gain in SDR over the CS-Mapping with BP.[4] In Fig. 5.4, the "Best least-square" decoding scheme (applied on the output $\hat{\mathbf{y}}$ of the Shannon-Kotel'nikov decoder) is also plotted as a reference. This decoding scheme requires additional side information as it assumes that the support I (i.e., the indices of the nonzero components in $\mathbf{u}$) is known a priori by the decoder. Hence, the best way to recover the source signal from the decoded measurement $\hat{\mathbf{y}}$ would be to apply the pseudo-inverse $(\mathbf{\Phi\Psi})_I^\dagger$ on the support, and set the remaining coordinates of $\mathbf{u}$ to zero.

In what follows, we summarize the results of our study of the sensitivity of the CS-Mapping and CS-BPDN system against mismatch in noise level. As in several applications, the encoder has no knowledge on the actual noise variance and a design noise level is assumed. However, the decoder can be designed to operate at the actual noise level provided the receiver can estimate the channel condition. The CS-BPDN system uses an uncoded linear system at the transmitter side which make it less sensitive to noise mismatch.

For the proposed system, as shown in Fig. 5.5, we notice that for low and moderate design TSNR levels, the mismatch in system SDR is insignificant when the actual TSNR is lower than the design TSNR level (TSNR_D). In contrast, when the actual

[4]The number of measurements is optimized for CS-Mapping with BP.

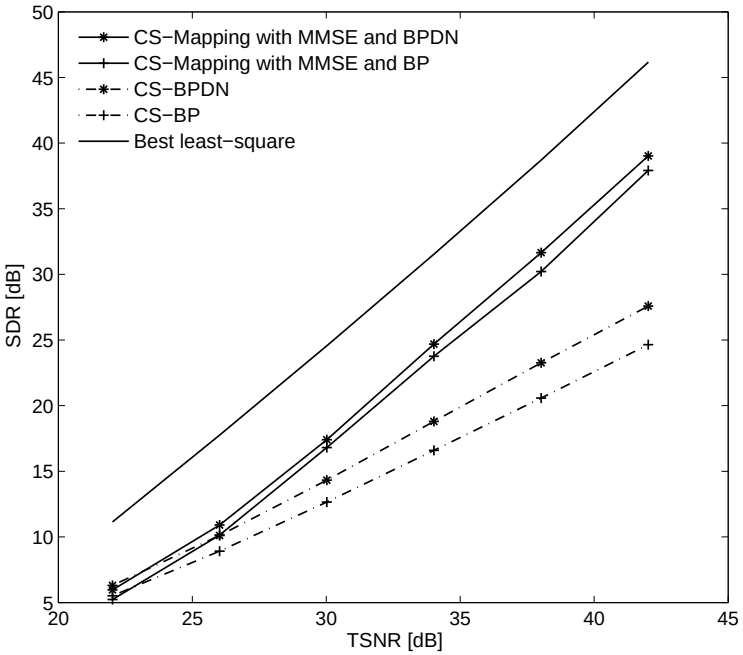

Figure 5.4: Performance of CS-Mapping and CS-BPDN with sparsity level $K = 6$ and signal length $N = 100$. The graph is made for $u_i \sim \mathcal{N}(0, 1)$. The number of measurements used by CS-Mapping at the asterisk marks are: [38 38 42 42 42 42], which correspond to the following CSNR[dB] levels: [3.2 7.2 10.7 14.7 18.7 22.7]. The performance of CS-BP is also shown for comparison.

TSNR$>$ TSNR$_D$, a $2 \sim 3$ dB loss in system SDR is noticed for each 4 dB mismatch in TSNR. For high TSNR$_D$, the proposed system is highly sensitive when the actual TSNR is lower than TSNR$_D$. Whereas, when the actual TSNR is greater than TSNR$_D$, the system SDR does not suffer from leveling-off effect and increases linearly with TSNR– for instance, an increase of 1 dB in TSNR results in a 1 dB increase in SDR. This trend is due to the analog nature of the proposed system. It is important to note that when the proposed system is designed for moderate to high TSNR, it will certainly perform better than the CS-BPDN when actual TSNR is greater than the designed one. Hence, it might be better to design the proposed system for the

highest expected channel noise. But at the same time, the gain from using the proposed system over CS-BPDN will decrease. Finally, it needs to be mentioned that the proposed purely-analog system is quite robust against a reasonable mismatch in channel noise.

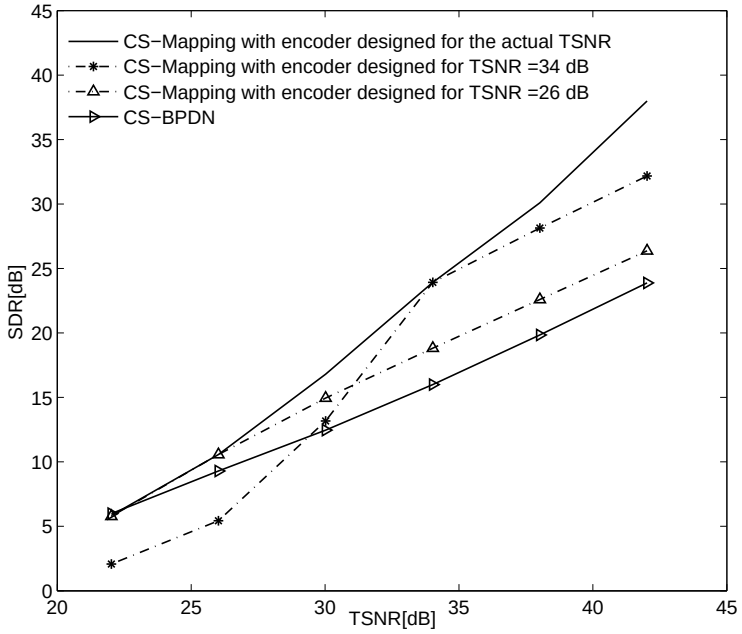

Figure 5.5: Performance of CS-Mapping where the encoder and decoder are, respectively, designed for the given TSNR and actual TSNR. The CS-Mapping and CS-BPDN optimized for each TSNR levels are also plotted. MMSE decoder and BPDN are used with CS-Mapping. The graph is made for signal length $N = 100$, sparsity level $K = 6$, and $u_i \sim \mathcal{N}(0, 1)$.

5.5 Summary and Conclusion

In this chapter, we have presented a system which combines compressed sensing and bandwidth expansion using Shanon-Kotel'nikov mapping in the presence of noise. The

proposed purely-analog system is optimized for minimal end-to-end distortion under a transmission power constraint. Simulation results have shown that the system outperforms the conventional CS system that assumes noiseless environment and a CS-based system that accounts for channel noise at the decoder. Note that one can also use the source-channel mappings of Chapter 3 and 4 in CS context for different rate targets.

Chapter 6

Conclusions

This chapter summarizes the major contributions in this thesis. All systems studied in the previous chapters are based on the $1:2$ double Archimedes' spiral. First, we combine the spiral mapping with multiple stage quantizers to achieve high (integer) expansion ratio. Then, the uncoded transmission and the spiral mapping are used to obtain a low (fractional) expansion ratio between 1 and 2. Finally, the $1:2$ spiral mapping is used within the compressive sensing context to increase immunity against channel noise. The main contributions can be summarized as follows

- In Chapter 3, a hybrid digital-analog source-channel coding with $1:3$ bandwidth expansion is proposed. The system parameters are numerically optimized to minimize the overall distortion. Moreover, an upper bound on the end-to-end system distortion is derived. Furthermore, we generalize the system to achieve higher expansion ratios $1:M$ (where the integer $M > 3$) by using multiple stage quantizers.

- In Chapter 4, a purely analog joint source-channel coding is presented. This

system is a $N : M$ bandwidth expansion scheme as long as the condition $N < M < 2N$ is fulfilled. Power is optimally allocated to minimize the overall distortion.

- In Chapter 5, a $1 : 2$ Shannon-Kotel'nikov mapping is applied in the compressed sensing context to increase the CS system's immunity against channel noise. The number of linear measurements is optimized to minimize the overall MSE distortion. The proposed scheme is compared with a CS-based system which accounts for channel noise during signal reconstruction.

All source-channel mappings proposed in this thesis can be used where low complexity and low delay are crucial constraints. Some applications can be found in wireless sensors networks, feedback channels, and closed-loop control. Finally, it is worth to investigate some of these mappings for sources with memory which is left for future work.

Bibliography

[1] C. E. Shannon, "Communication in the presence of noise," in *Proc. IRE*, 1949, pp. 10–21.

[2] K. H. Lee and D. P. Petersen, "Optimal linear coding for vector channels," *IEEE Trans. Communications*, vol. COM-24, no. 12, pp. 1283–1290, 1976.

[3] C. E. Shannon, "A mathematical theory of communication," *The Bell System Technical Journal*, vol. 27, pp. 379–423, 1948.

[4] T. M. Cover and J. A. Thomas, *Elements of Information Theory*, Wiley, New York, 2006.

[5] N. Farvardin and V. Vaishampayan, "On the performance and complexity of channel-optimized vector quantizers," *IEEE Trans. Information Theory*, vol. 37, pp. 155–159, Jan 1991.

[6] V. A. Vaishampayan, *Combined Source-Channel Coding for Bandwidth Waveform Channels*, Ph.D. dissertation, University of Maryland, 1989.

[7] S.-Y. Chung, *On the Construction of Some Capacity-Approaching Coding Schemes*, Ph.D. dissertation, Massachusetts Institute of Technology, Sept. 2000.

[8] T. A. Ramstad, "Shannon mappings for robust communication," *Telektronikk*, vol. 98, no. 1, pp. 114–128, 2002.

[9] D. Donoho, "Compressed sensing," *IEEE Trans. Information Theory*, vol. 52, no. 4, pp. 1289–1306, Apr 2006.

[10] S. S. Chen, D. L. Donoho, and M. A. Saunders, "Atomic decomposition by basis pursuit," *SIAM Journal on Scientific Computing*, vol. 20, no. 1, pp. 31–61, 1998.

[11] S. Mallat and Z. Zhang, "Matching pursuits with time-frequency dictionaries," *IEEE Trans. Signal Processing*, vol. 41, no. 12, pp. 3397–3415, Dec 1993.

[12] A. Fuldseth and T. A. Ramstad, "Bandwidth compression for continuous amplitude channels based on vector approximation to a continuous subset of the source signal space," in *Proc. IEEE International Conference on Acoustic, Speech, Signal Processing (ICASSP)*, April 1997.

[13] A. Fuldseth, *Robust Subband Video Compression for Noisy Channels with Multilevel Signaling*, Ph.D. dissertation, Norwegian University of Science and Technology, 1997.

[14] P. A. Floor, T. A. Ramstad, and N. Wernersson, "Power constrained channel optimized vector quantizers used for bandwidth expansion," in *Proc. IEEE International Symp. Wireless Commun. Syst.*, Trondheim, Norway, Oct 2007.

[15] V. A. Kotel'nikov, *The Theory of Optimum Noise Immunity*, McGraw-Hill, New York, 1959.

[16] T. Berger and D. W. Tufts, "Optimum pulse amplitude modulation part I: transmitter-receiver design and bounds from information theory," *IEEE Trans. Information Theory*, vol. IT-13, no. 2, pp. 196–208, Apr 1967.

[17] F. Hekland, P. A. Floor, and T. A. Ramstad, "Shannon-Kotel'nikov mappings in joint source-channel coding," *IEEE Trans. Communications*, vol. 57, no. 1, pp. 94–105, Jan 2009.

[18] F. Hekland, G. E. Oien, and T. A. Ramstad, "Using 2:1 Shannon mapping for joint source-channel coding," in *Proc. Data Compression Conference DCC*, Snowbird, UT, Mar 2005, pp. 223–232.

[19] F. Hekland, *On the Design and Analysis of Shannon-Kotel'nikov Mappings for Joint Source-Channel Coding*, Ph.D. dissertation, Norwegian University of Science and Technology, 2007.

[20] P. A. Floor, *On the Theory of Shannon-Kotel'nikov Mappings in Joint Source-Channel Coding*, Ph.D. dissertation, Norwegian University of Science and Technology, 2008.

[21] U. Mittal and N. Phamdo, "Hybrid digital analog (HDA) joint source channel codes for broadcasting and robust communications," *IEEE Trans. Information Theory*, vol. 48, pp. 1082–1102, May 2002.

[22] M. Skoglund, N. Phamdo, and F. Alajaji, "Hybrid digital-analog source-channel coding for bandwidth compression/expansion," *IEEE Trans. Information Theory*, vol. 52, no. 8, pp. 3757–3763, Aug 2006.

[23] M. Skoglund, N. Phamdo, and F. Alajaji, "Design and performance of VQ-based hybrid digital-analog joint source-channel codes," *IEEE Trans. Information Theory*, vol. 48, no. 3, pp. 708–720, Mar 2002.

[24] H. Coward and T.A. Ramstad, "Hybrid digital-analog transmission of analog source signals," in *Norwegian Signal Processing Symposium*, Sem Gjestegrd Asker, Norway, Sep 1999.

[25] H. Coward and T.A. Ramstad, "Quantizer optimization in hybrid digital-analog transmission of analog source signals," in *Proc. IEEE International Conference on Acoustics, Speech, and Signal Processing*, 2000, pp. 2637–2640.

[26] Y. Wang, F. Alajaji, and T. Linder, "Hybrid digital-analog coding with bandwidth compression for gaussian source-channel pairs," *IEEE Trans. Communications*, vol. 57, no. 4, pp. 997–1012, April 2009.

[27] D. Sakrison, *Communication Theory: Transmission of Waveforms and Digital Information*, John Wiley & Sons Inc, 1968.

[28] Y. Hu, J. Garcia-Frias, and M. Lamarca, "Analog joint source channel coding using space-filling curves and MMSE decoding," in *Proc. Data Compression Conference DCC*, Snowbird, UT, Mar 2009, pp. 103–112.

[29] H. Coward, *Joint Source-Channel Coding: Development of Methods and Utilization in Image Communication*, Ph.D. thesis, Norwegian University of Science and Technology, 2001.

[30] M. Kleiner and B. Rimoldi, "Asymptotically optimal joint source-channel coding with minimal delay," in *Proc. IEEE Global Telecommunications Conference*, Honolulu, HI, 2009.

[31] Y. Hu and J. Garcia-Frias, "Optimizing power allocation in analog joint source-channel coding," in *Proc. 43rd Annual Conference on Information Sciences and Systems CISS*, Baltimore, MD, Mar 2009, pp. 72–76.

[32] T. J. Goblick, "Theoretical limitations on the transmission of data from analog sources," *IEEE Trans. on Information Theory*, vol. 11, pp. 558–567, Oct 1965.

[33] W. Bajwa, J. Haupt, A. Sayeed, and R. Nowak, "Compressive wireless sensing," in *The Fifth International Conference on Information Processing in Sensor Networks (IPSN)*, Nashville, TN, 2006, pp. 134–142.

[34] N. Wernersson, M. Skoglund, and T. Ramstad, "Polynomial based analog source-channel codes," *IEEE Trans. Communications*, vol. 57, pp. 2600–2606, Sept 2007.

[35] A.N. Kim and F. Hekland, "Dimension reduction and expansion: Distributed source coding in a noisy environment," in *Proc. Data Compression Conference DCC*, Snowbird, UT, Mar 2008, pp. 332–341.

[36] E. Candes, J. Romberg, and T. Tao, "Stable signal recovery from incomplete and inaccurate measurements," *Communications on Pure and Applied Mathematics*, vol. 59, no. 8, pp. 1207–1223, 2006.

[37] E. Candes, J. Romberg, and T. Tao, "Robust uncertainty principles: Exact signal reconstruction from highly incomplete frequency information," *IEEE Trans. Information Theory*, vol. 52, no. 2, pp. 489–509, Feb 2006.

[38] E. Candes and T. Tao, "Near optimal signal recovery from random projections: Universal encoding strategies?," *IEEE Trans. Information Theory*, vol. 52, no. 12, pp. 5406–5425, Dec 2006.

[39] E. J. Candes and M. B. Wakin, "An introduction to compressive sampling," *IEEE Signal Processing Magazine*, pp. 21–30, Mar. 2008.

[40] J. A. Tropp and A. C. Gilbert, "Signal recovery from random measurements via orthogonal matching pursuit," *IEEE Trans. Information Theory*, vol. 53, pp. 4655–4666, 2007.

[41] R. Tibshirani, "Regression shrinkage and selection via the lasso," *J. Roy. Stat. Soc. Ser. B*, vol. 58, no. 1, pp. 267–288, 1996.